COMPARISONS OF POINT AND AVERAGE CAPILLARY PRESSURE - SATURATION FUNCTIONS FOR POROUS MEDIA

A Dissertation Presented for the
Doctor of Philosophy
Degree
The University of Tennessee, Knoxville

Samuel Clark Cropper
December 2014

DEDICATION

This dissertation is dedicated to my wife Cheri, and my children Mason and Grace. You are blessings beyond anything I could have imagined for myself.

ACKNOWLEDGEMENTS

My first thank you goes to the people who graciously allowed me to postpone or re-schedule previous commitments so I could pursue this research. More than anyone else I thank my wife Cheri. She provided encouragement, inspiration, and shouldered extra responsibilities to make our home function well during my research. I also thank my daughter Grace, and my son Mason for their many encouragements and inspiration. I could not ask for a more supportive family. Nancy Morris, Dean of the Math and Science Division at Volunteer State Community College, played the critical role of finding ways for me to meet my obligations to the college while also meeting my research schedule. Similarly, Dr. Robert Carter, Science Chair at Volunteer State Community College, worked with me to coordinate my teaching loads around my research schedule. Without the enthusiastic cooperation of my family and these colleagues I could not have met these obligations while also completing this research.

Making time for research is only the beginning. The research itself would not be possible without the support of the faculty members who guided me through the research process. First on this list is my advisor Dr. Edmund Perfect. I am deeply grateful to him for taking on a part-time student, for his advice during development of my research topic, and his encouragement and patience throughout the work. His critical reviews and advice on the work were always timely and insightful. I also thank the other members of my committee Dr. Larry McKay, Dr. Melanie Mayes, and Dr. Jaehoon Lee, for help navigating the academic process and their editorial comments to improve this document. I also thank post-doctoral researcher Dr. Chu-Lin Cheng for sharing his expertise with the STOMP simulator and several good pieces of advice during the early phases of my research.

Finally, I would like to thank the taxpayers of the State of Tennessee. I benefited greatly from academic fee waivers provided to me as an employee of a public higher education institution in Tennessee.

ABSTRACT

The relationship between the volume of water occupying pores in soil or rock and its energy state is called the capillary pressure–saturation function. This is an important hydrogeologic property needed for modeling multiphase flow and transport. Standard methods used to determine capillary pressure–saturation behavior produce volume averaged functions rather than point functions. Average functions can produce erroneous simulations in flow models. Analytical expressions permit extraction of point functions from average functions, and predictions of average functions from point function parameters. These concepts are discussed in Chapter I.

Chapter II compares average and point functions from centrifugation of Berea sandstone, glass beads, and Hanford sediments. The averaging method smoothed out the drainage process, yielding less steep capillary pressure-saturation functions compared to the point functions. Maximum deviations in saturation between the two methods ranged from 0.08 to 0.28 cm^3 [cubic centimeters] cm^{-3}, and generally occurred at low suctions. These discrepancies can lead to inaccurate predictions of hydraulic properties.

Chapter III presents numerical simulations of CO_2 [carbon dioxide] injection into saline aquifers for geologic sequestration. Average function parameters were compared to point parameters. Simulations using point parameters have injection flow rates 1.36 times faster than the injection flow rates produced by simulations based on the average parameters. The cost of CO_2 injected at a gas pressure of 1.5 x 10^7 Pa [Pascals] was \$0.87 [0.87 dollars] per ton using the average parameter set and \$0.65 per ton of CO_2 injected using the point parameter set.

Chapter IV evaluates analytical expressions that relate point functions to average functions. These expressions can extract point parameters from average functions, and estimate average functions from point parameters. Average functions for nine columns of Flint sand between 4.3 cm and 55.0 cm tall were predicted from point functions and compared to average functions measured using the hanging

water column method. Agreement was generally good. Predictions of point parameters from observed average retention data produced variable results compared to point parameters measured by neutron imaging. Chapter V summarizes results from the preceding three chapters and provides some suggestions for future research.

TABLE OF CONTENTS

Chapter I Introduction 1
References 6
Chapter II Comparison of Average and Point Capillary Pressure-Saturation Functions Determined by Steady-State Centrifugation 8
Abstract 10
Introduction 11
Materials and Methods 14
Sample Preparation 14
Centrifugation 16
Data Analysis 17
Results and Discussion 19
References 25
Appendix II-A Tables 29
Appendix II-A Figures 35
Chapter III Modeling the Impact of Capillary Pressure – Saturation Parameters on Geologic Carbon Sequestration Simulations 43
Abstract 45
Introduction 46
Materials and Methods 48
Petrophysical Properties 48
STOMP Simulation Scenario 48
Data Analysis 49
Results and Discussion 49
Point Simulations Compared to Average Simulations 49
The Impact of Flow Rate on Injection Cost Estimates 50
Conclusions 51
References 52
Appendix III-A Tables 54
Appendix III-B Figures 58
Chapter IV Comparison of Upscaled and Measured Capillary Pressure – Saturation Parameters for Flint Sand 59
Abstract 61
Introduction 62
Materials and Methods 65
Hanging Water Column Experiments 65
Neutron Point BC Parameterization 66
BC-vG Upscaler Predicted vGE Average Functions 67
TrueCell Point BC Parameterization 68
Results and Discussion 68
Hanging Water Column Experiments 68
Forward Predictions of Average vGE Parameters from Point Parameters 69

Inverse Predictions of Point Parameters from Average Data 72
Discussion and Conclusions 73
References 77
Appendix IV-A Tables 79
Appendix IV-B Figures 86
Chapter V Conclusions 97
Vita 101

LIST OF TABLES

Table 1. Physical properties of median grain diameter (d50), porosity (ϕ), and saturated hydraulic conductivity (K_{sat}) for the Berea sandstone, glass beads (GB), and disturbed (HL) and undisturbed upper coarse layer (UCL), middle fine layer (MFL), and lower course layer (LCL) Hanford sediments investigated. 29
Table 2. Number and duration (t) of constant angular velocity (ω) periods used in the centrifuge experiments with Berea sandstone, glass beads (GB), and disturbed (HL) and undisturbed upper course layer (UCL), middle fine layer (MFL), and lower coarse layer (LCL) Hanford sediments. 30
Table 3. Summary of van Genuchten (1980) model fits and estimates of the residual saturation, S_r, and α and n parameters for the averaging method of Reatto et al. (2008) for the Berea sandstone, glass beads (GB), and disturbed (HL) and undisturbed upper coarse layer (UCL), middle fine layer (MFL), and lower coarse layer (LCL) Hanford sediments..... 31
Table 4. Summary of van Genuchten (1980) model fits and estimates of the residual saturation, S_r, and α and n parameters for the integral method of Bentsen and Anli (1977) for the Berea sandstone, glass beads (GB), and disturbed (HL) and undisturbed upper coarse layer (UCL), middle fine layer (MFL), and lower course layer (LCL) Hanford sediments..... 32
Table 5. Summary of Brooks and Corey (1964) model fits and estimates of the residual saturation S_r, air-entry value ψa, and pore-size distribution index λ for the integral method of Bentsen and Anli (1977) for the Berea sandstone, glass beads (GB), and disturbed (HL) and undisturbed upper coarse layer (UCL), middle fine layer (MFL), and lower coarse layer (LCL) Hanford sediments. 33
Table 6. Maximum deviations in relative saturation (ΔS) between the averaging and integral methods for the Brooks-Corey (BC) or van Genuchten (VG) models for the Berea sandstone, glass beads (GB), and disturbed (HL) and undisturbed upper coarse layer (UCL), middle fine layer (MFL), and lower coarse layer (LCL) Hanford sediments. 34
Table 7. Physical properties of porosity (ϕ), and intrinsic permeability (k) for the Berea sandstone cores..... 54
Table 8. Summary of van Genuchten (1980) estimates of the residual saturation, S_r, and α, n, and m parameters for the average and point methods fit to centrifuge retention data for Berea sandstone core samples (Cropper et. al, 2011). 55
Table 9. Mean gas pressures corresponding with each simulated injection flow rate for the point and average simulation sets. 56
Table 10. Injection flow rates, mass of CO_2 injected per day, and dollars per ton of CO_2 injected compared for two simulation parameter sets injected at mean gas pressures of 1.5×10^7 Pa. 57
Table 11. Physical properties of length, bulk density, and porosity, and transducer log interval time for Flint sand hanging water columns. 79

Table 12. Range of capillary pressure, number of equilibrium steps, and total drainage time for Flint sand hanging water columns. 80
Table 13. Summary of Brooks and Corey (1964) model fits and estimates of the saturation (S), residual saturation S_r, air-entry value ψ_a, and pore-size distribution index λ fit to 1080 retention data points in Flint sand determined by neutron imaging (Kang et al, 2014). 81
Table 14. Summary of van Genuchten (1980) parameters predicted by the BC-vG Upscaler based on neutron point parameters and column length. 82
Table 15. Summary of van Genuchten (1980) parameters estimated from the measured average capillary pressure-saturation data for each Flint sand column. 83
Table 16. Summary of van Genuchten (1980) parameters predicted by the BC-vG Upscaler algorithm based on neutron point parameters, column length, and a top reference for pressure. 84
Table 17. Summary of Brooks and Corey (1964) parameters of the saturation (S), residual saturation S_r, air-entry value ψ_a, and pore-size distribution index λ estimated by TrueCell (Jalbert et. al, 1999) from average capillary pressure-saturation data from nine columns of Flint sand. Neutron imaging point BC parameters are included for comparison. 85

LIST OF FIGURES

Figure 1. Step changes in centrifuge angular velocity, ω (lower curve), and corresponding water outflow, Q_w (upper curves), through time for the three replicate samples of Berea sandstone. 35
Figure 2. Measured capillary pressure-saturation data and fitted van Genuchten (1980) function for the Berea-1 sandstone sample based on the averaging method of Reatto et al. (2008). 36
Figure 3. Measured and modeled average saturations and resulting point van Genuchten (1980) capillary pressure-saturation function for the Berea-1 sandstone sample based on the integral method of Bentsen and Anli (1977)... 37
Figure 4. Relationship between residual saturation (S_r) values in the van Genuchten (1980) capillary pressure-saturation equation estimated using the averaging and integral methods. The dashed line indicates a 1:1 correspondence. 38
Figure 5. Relationship between the α parameter in the van Genuchten (1980) capillary pressure-saturation equation estimated using the averaging and integral methods. The dashed line indicates a 1:1 correspondence. 39
Figure 6. Relationship between the n parameter in the van Genuchten (1980) capillary pressure-saturation equation estimated using the averaging and integral methods. The dashed line indicates a 1:1 correspondence. 40
Figure 7. Measured and modeled average saturations and resulting point Brooks and Corey (1964) capillary pressure-saturation function for the Berea-1 sandstone sample based on the integral method of Bentsen and Anli (1977). 41
Figure 8. Comparison of capillary pressure-saturation function for the Berea-1 sample obtained using the averaging and integral methods..... 42
Figure 9. Comparison of mean gas pressures resulting from simulations using average simulation parameters and mean gas pressure resulting from simulations using point simulation parameters at eight injection flow rates. 58
Figure 10. Conceptual diagram showing relationships between experimental data, data processing and parameterizations, and comparisons between experimental observations and predictions from analytical expressions. 86
Figure 11. Hanging water column laboratory setup showing sand column, burette, pressure transducer, and data logging computer. 87
Figure 12. Cumulative water outflow through time for the 23.8 cm, 19.7 cm, and 24.9 cm Flint sand hanging water column drainage experiments. 88
Figure 13. Comparison of upscaled predictions of capillary pressure-saturation functions (red) with measured average data points (blue) and van Genuchten (1980) functions fitted to measured average data points (green) for nine column lengths of Flint sand. 89
Figure 14. Relationship between observed relative saturation values and estimations of relative saturation in the van Genuchten (1980) capillary pressure-saturation equation predicted by the BC-vG Upscaler. The dashed line indicates a 1:1 correspondence. 90

Figure 15. Relationship between α parameters, n parameters, residual saturation (S_r) values, and saturation values (S) in the van Genuchten (1980) capillary pressure-saturation equation predicted by the BC-vG Upscaler and fitted to the measured average drainage data. The dashed line indicates a 1:1 correspondence. 91
Figure 16. Comparisons of bottom (red), middle (green), and top (blue) pressure references on upscaled predictions of the capillary pressure-saturation functions for the nine column lengths..... 92
Figure 17. Upscaled top-pressure reference predictions of average capillary pressure saturation functions (orange) compared with measured average data points (blue) and van Genuchten (1980) functions fitted to measured average data points (green) for nine column lengths of Flint sand. Red lines are uncorrected mid-reference BCvG Upscaler predictions repeated here to for comparison with corrected top-reference BCvG Upscaler predictions. 93
Figure 18. Relationship between observed relative saturation values and estimations of relative saturation in the van Genuchten (1980) capillary pressure-saturation equation predicted by the BC-vG Upscaler with the pressure reference at the column top. The dashed line indicates a 1:1 correspondence. 94
Figure 19. Relationship between α parameters, n parameters, residual saturation (S_r) values, and saturation values (S) in the van Genuchten (1980) capillary pressure-saturation equation predicted by the BC-vG Upscaler and fitted to the measured average drainage data. The dashed line indicates a 1:1 correspondence. 95
Figure 20. Relationship between TrueCell (Jalbert et. al, 1999) estimates of residual saturation (S_r) parameters, air entry (ψ_a) parameters, and pore size distribution index (λ) parameters shown as circles, and parameter values determined by neutron imaging. Neutron imaging values are shown as dashes with 95% confidence limits as error bars (gray)..... 96

Chapter I

Introduction

The volume of water occupying pores in soil or rock is a function of the energy state of the soil water. Both the volume of water and the energy state may be referred to by various names. The volume of water can be expressed as water content (percentage of the total volume occupied by water), or saturation (percentage of the porosity occupied by water). The energy state can be described as matric potential (negative values with units of kPa or cm) or capillary pressure, tension, or suction (positive values with units of kPa or cm). As a result, the relationship may be called the capillary-pressure saturation function, the water retention curve, the water characteristic curve, or others depending on the application or study area (Dane and Hopmans, 2002). In this document, the relationship will be called the capillary pressure-saturation function and abbreviated as $S(\psi)$, where S is relative saturation and ψ is capillary pressure. Whichever terminology is used, the relationship is a fundamental hydraulic property of variably-saturated rock and soils. It is needed for simulations of multiphase flow and chemical transport in porous media, as well as to predict relative permeability. It also has relevance to important agricultural, environmental and energy related applications such as crop production, enhanced oil recovery, subsurface carbon sequestration, and remediation of contaminated soils.

The capillary-pressure saturation function, $S(\psi)$, can be measured directly at a physical point. This requires paired saturation and capillary pressure determinations at a physical point within a sample. For example, Sakaki and Illangasekare (2007) measured point capillary pressure-saturation functions using a time domain reflectometry (TDR) probe in conjunction with a hanging water column. Vasin et al. (2008), Cheng et al. (2012), and Kang et al. (2014) all employed neutron radiography in conjunction with a hanging water column to measure $S(\psi)$ functions at sample points. Unfortunately, these direct methods are not commonly used to characterize capillary pressure-saturation functions because they require more sophisticated technology and are more expensive. More commonly, the capillary-pressure saturation function is determined at a local scale experimentally by observing changes in saturation of a sample of finite length as it is subjected to a series

of step changes in pressure in a pressure cell, hanging water column, or centrifuge. These methods are relatively simple, fast, and inexpensive. If the densities of the non-wetting and wetting fluids are different, the pressure, ψ will vary with height within the porous medium (Dane et al., 1992; Liu and Dane, 1995a). Thus for the most common experimental methods, any particular data point in the measured capillary-pressure saturation function relates the average saturation of the sample to an energy state (capillary pressure) applied at a point within the sample. When the sample height is small, variations are also small, but short samples are not always representative of the material. Thus, when tall samples are used for measurement, the saturation of the sample at the point where ψ is controlled, S, can deviate significantly from the measured <S>.

Use of the average capillary pressure-average saturation function, <S>(ψ), instead of the point capillary pressure-saturation function, S(ψ), in flow and transport models can produce erroneous predictions (Peters and Durner, 2006). Even relatively small variations in capillary pressure-saturation function parameters can produce large differences in flow simulations (Cheng et. al, 2013). Because of potential scale dependent deviations, Dane and Hopmans (2002) recommended applying a correction to extract the point, S(ψ), function from measured, <S>(ψ), functions if the sample is more than 3 cm in height. Sakaki and Illangasekare (2007) recommended applying a correction if the column height is longer than one third of the displacement air entry head. Liu and Dane (1995a,b), Jalbert et al. (1999), and Dane and Hopmans (2002) presented analytical expressions to derive point S(ψ), functions from measured average, <S>(ψ), functions, including a computer application, TrueCell (Jalbert et. al, 1999), that inversely corrects for the height of the sample given information about the pressure cell setup and fluid densities. Cheng et al. (2013) used the same analytical expressions to develop a computer program, the BC-vG Upscaler, that upscales point S(ψ) functions to predict the average, <S>(ψ), function at any scale of interest assuming the porous medium is homogeneous. Forward predictions of the BC-vG Upscaler have not yet been verified experimentally.

Capillary pressure-saturation functions can also be determined by centrifugation. Russell and Richards (1938) were the first to construct the entire capillary pressure-saturation function by centrifuging soil samples. However, their data were average, $\langle S \rangle(\psi)$, functions. Oden (1975) appears to have been the first to extract a point $S(\psi)$ function from centrifuge experiments performed on soil samples. According to Christiansen (2001) computational procedures applied to centrifuge drainage data can be divided into two main groups: differential and integral methods. Hassler and Brunner (1945) were the first to propose a method to calculate the point $S(\psi)$ function by differentiating the product of $\langle S \rangle$ and the point ψ. Numerical differentiation or fitting a differentiable equation to the observation data can also be used (Christiansen, 2001). The integral method uses a parametric expression for the point $S(\psi)$ function to predict S from known values of ψ at discrete points along the length of the sample. The resulting S values are numerically integrated to give the $\langle S \rangle$ for a given angular velocity (ω). The calculated $\langle S \rangle$ values are then compared to the measured $\langle S \rangle$ values and, using an iterative least-square minimization technique, the parameters of the point equation are optimized. This one-dimensional integral method was originally described by Bentsen and Anli (1977).

The following chapters contain results of several investigations into the relationship between point $S(\psi)$ and average $\langle S \rangle(\psi)$ functions. In Chapter II an integral computational method is applied to centrifuge drainage data to extract point $S(\psi)$ functions for a range of porous media including Berea sandstone, glass beads, and unconsolidated sediments. The resulting point $S(\psi)$ functions are then compared with average $\langle S \rangle(\psi)$ functions determined in the same materials. In Chapter III a model scenario is created using the STOMP (Subsurface Transport Over Multiple Phases) numerical modeling tool for injection of supercritical CO_2 into a deep formation for long term geologic carbon sequestration. The model is then used to compare simulations using point, $S(\psi)$, versus average, $\langle S \rangle(\psi)$, functions on CO_2 injection flow rate and operating efficiency. In Chapter IV analytical expressions relating point $S(\psi)$ and average $\langle S \rangle(\psi)$ functions are applied to drainage data from

columns of varying lengths of Flint sand. Point S(ψ) functions determined directly in Flint sand by neutron imaging are upscaled using the BC-vG Upscaler to predict average <S>(ψ) functions for columns of nine different lengths of Flint sand ranging from 4.3 cm to 55.0 cm. The hanging water column method is used to measure average <S>(ψ) functions in Flint sand columns for the same lengths. The forward predictions of average functions are compared to observed average functions. The observed drainage data are processed using TrueCell to inversely determine point S(ψ) functions from the observed data. These point functions are compared to the point function produced by neutron imaging. Finally, Chapter V presents some general conclusions along with some suggestions for future research.

References

Bentsen, R.G., and J. Anli. 1977. Using parameter estimation techniques to convert centrifuge data into a capillary–pressure curve. SPE J. 17:57–64.

Cheng, C. L., M. Kang, E. Perfect, S. Voisin, J. Horita, H. Z. Bilheux, J. M. Warren, D. L. Jacobson, and D. S. Hussey. 2012. Average soil water retention curves measured by neutron radiography. Soil Science Society of America Journal 76(4):1184-1191.

Cheng, C. L., et al. 2013. Sensitivity of injection costs to input petrophysical parameters in numerical geologic carbon sequestration models. International Journal of Greenhouse Gas Control 18: 277-284.

Christiansen, R.L. 2001. Two-phase flow through porous media. Colorado School of Mines, Boulder.

Dane, J.H., and J.W. Hopmans. 2002a. Introduction. p. 671–673. In J.H. Dane and G.C. Topp (ed.). Methods of soil analysis. Part 4. Physical methods. SSSA Book Ser. 5. SSSA, Madison, WI

Dane, J.H., and J.W. Hopmans. 2002b. Samples. p. 676–677. In J.H. Dane and G.C. Topp (ed.). Methods of soil analysis. Part 4. Physical methods. SSSA Book Ser. 5. SSSA, Madison, WI

Dane, J.H., and J.W. Hopmans. 2002c. Computational Corrections. p. 714–717. In J.H. Dane and G.C. Topp (ed.). Methods of soil analysis. Part 4. Physical methods. SSSA Book Ser. 5. SSSA, Madison, WI

Dane, J.H., M. Oostrom, and B.C. Missildine. 1992. An improved method for the determination of capillary pressure–saturation curves involving TCE, water and air. J. Contam. Hydrol. 11:69–81.

Hassler, G.L., and E. Brunner. 1945. Measurement of capillary pressures in small core samples. Trans. Am. Inst. Min. Metall. Pet. Eng. 160:114–123.

Jalbert, M., J.H. Dane, and J.H. Liu. 1999. TrueCell: Physical point Brooks–Corey parameters using pressure cell data. Users guide for version 1.2. Spec. Rep. Dep. of Agron. and Soils, Auburn Univ., Auburn, AL.

Kang, M., E. Perfect, C. L. Cheng, H. Z. Bilheux, J. Lee, J. Horita, and J. M. Warren. 2014. Multiple pixel-scale soil water retention curves quantified by neutron radiography. Advances in Water Resources 65:1-8.

Liu, H.H., and J.H. Dane. 1995a. Improved computational procedure for retention relations of immiscible fluids using pressure cells. Soil Sci. Soc. Am. J. 59:1520–1524.

Liu, H.H., and J.H. Dane. 1995b. Computation of the Brooks–Corey parameters at a physical point based on pressure cell data. Spec. Rep. Dep. of Agron. and Soils, Auburn Univ., Auburn, AL.

Odén, S. 1975. An integral method for the determination of moisture retention curves by centrifugation. Grundfoerbaettring 27:137–143.

Peters, A., and W. Durner. 2006. Improved estimation of soil water retention characteristics from hydrostatic column experiments. Water Resour. Res. 42:W11401, doi: 10.1029/2006WR004952.

Russell, M.B., and L.A. Richards. 1938. The determination of soil moisture energy relations by centrifugation. Soil Sci. Soc. Am. Proc. 3:65–69.

Sakaki, T., and T.H. Illangasekare. 2007. Comparison of height-averaged and point measured capillary pressure–saturation relations for sands using a modified Tempe cell. Water Resour. Res. 43:W12502, doi:10.1029/2006WR005814.

Vasin, M., Lehmann, P., Kaestner, A., Hassanein, R., Nowak, W., Helmig, R., & Neuweiler, I. 2008. Drainage in heterogeneous sand columns with different geometric structures. Advances in Water Resources, 31(9):1205-1220.

Chapter II

Comparison of Average and Point Capillary Pressure-Saturation Functions Determined by Steady-State Centrifugation

A version of this chapter was originally published by S.C. Cropper, E. Perfect, E.H. van den Berg, and M.A. Mayes:

Cropper, S.C., E. Perfect, E.H. van den Berg, and M.A. Mayes. 2011. Comparison of average and point capillary pressure-saturation functions determined by steady-state centrifugation. Soil Sci. Soc. Am. J. 75:17-25.

Samuel Clark Cropper contributed to this chapter by performing data analysis and writing the paper. Others contributed by collecting samples, running the centrifugation experiments, and revising the manuscript.

Abstract

The capillary pressure-saturation function can be determined from centrifuge drainage experiments. In soil physics, the data resulting from such experiments are usually analyzed by the "averaging method." In this approach, average relative saturation, <S>, is expressed as a function of average capillary pressure, <ψ>, i.e. <S>(<ψ>). In contrast, the capillary pressure - saturation function at a physical point, i.e., S(ψ), has been extracted from similar experiments in petrophysics using the "integral method." The purpose of this paper is to introduce the integral method to a soil physics audience, and to compare S(ψ) and <S>(ψ) functions, as parameterized by the Brooks and Corey and van Genuchten equations, for 16 samples drawn from a range of porous media (i.e., Berea sandstone, glass beads, Hanford sediments). Steady-state centrifuge experiments were performed on pre-consolidated samples with a URC-628 Ultra-Rock Core centrifuge. The angular velocity and water production data sets were then analyzed using both the averaging and integral methods. The results show that the averaging method smoothes out the drainage process, yielding less steep capillary pressure - saturation functions relative to the corresponding point-based curves. Maximum deviations in saturation between the two methods ranged from 0.08 to 0.28, and generally occurred at low suctions. These discrepancies can lead to inaccurate predictions of other hydraulic properties such as the relative permeability function. Therefore, we strongly recommend use of the integral method instead of the averaging method when determining the capillary pressure - saturation function by steady-state centrifugation. This method can be successfully implemented using either the van Genuchten or Brooks and Corey functions, although the later provides a more physically precise description of air entry at a physical point.

Introduction

The capillary pressure-saturation function is an important hydraulic property of variably-saturated rocks and soils. This function is needed for simulating multiphase fluid flow and chemical transport in porous media in applications such as agricultural crop production, enhanced oil recovery, subsurface carbon sequestration, and remediation of contaminated soils. In soil physics, the capillary pressure - saturation function is traditionally determined in the laboratory using a hanging water column (Dane and Hopmans, 2002a) and/or pressure plates (Dane and Hopmans, 2002b). In these methods, a series of capillary pressures, ψ, are imposed at a particular point and the corresponding volumetric water contents for the entire porous medium, $<\theta>$, are determined gravimetrically or manometrically. If the densities of the non-wetting and wetting fluids are different, ψ will vary with height within the porous medium (Dane et al., 1992; Liu and Dane, 1995a). As a result, the volumetric water content at the point where ψ is controlled, θ, can deviate significantly from the measured $<\theta>$. Thus, use of the capillary pressure-average saturation function, $<\theta>(\psi)$, instead of the point capillary pressure-saturation function, $\theta(\psi)$, in flow and transport models can produce erroneous predictions of important hydraulic properties such as the relative permeability function (Peters and Durner, 2006).

Because point measurements of θ are rarely available in hanging water column and pressure plate experiments, computational procedures have been developed to extract the $\theta(\psi)$ function from the measured $<\theta>(\psi)$ function. Liu and Dane (1995a,b), Jalbert et al. (1999), and Dane and Hopmans (2002c) presented analytical expressions to account for variations in ψ with column height. Their approach, called TrueCell, corrects the parameters of the Brooks and Corey (1964) equation for the height of the experimental column given information about the pressure cell setup and fluid densities. Sakaki and Illangasekare (2007) tested TrueCell against independent measurements of $\theta(\psi)$ made at a specific point in nine columns of sandy material. Jalbert and Dane (2001) proposed an alternative

correction procedure that does not require the assumption of a particular equation for the $\theta(\psi)$ function. Because it is based on numerical derivatives, however, the method is highly sensitive to small fluctuations in the experimental data (Perfect et al, 2004). Despite these limitations, Tokunaga et al. (2002) were able to apply a special case of this procedure to obtain $\theta(\psi)$ functions for gravels. Schroth et al. (1996) introduced a more robust integral method to correct the parameters of the van Genuchten (1980) equation for column height. A numerical scheme was used to predict the $<\theta>$ with the parameters of the point function estimated by least squares optimization against the measured $<\theta>$ values. Peters and Durner (2006) generalized the numerical approach for arbitrary capillary pressure-saturation functions, including bimodal functions.

There is long history in soil physics of using centrifuges to determine the capillary pressure - saturation function. Briggs and McLane (1907) were the first use steady-state centrifugation to manipulate the water content of soil samples in drainage experiments. Later, Gardner (1937) measured ψ by determining the equilibrium water content of calibrated filter papers placed in contact with moist soil. The filter papers were calibrated by determining their water contents following equilibration at different angular velocities in a centrifuge. Russell and Richards (1938) were the first to construct the entire capillary pressure - saturation function by centrifuging soil samples. However, their data are actually $<\theta>(\psi)$ functions. Khanzode et al. (2002) used essentially the same method to analyze their centrifuge data. The most recent approach has been to average the variation in ψ within the centrifuged sample, resulting in an average capillary pressure-average saturation function, $<\theta>(<\psi>)$ (Reatto et al., 2008). We refer to this method as the *averaging method*.

In contrast to the above studies, only two reports were found in the soil physics literature dealing with the integral method applied to centrifuge data. Oden (1975) appears to have been the first to extract a point $\theta(\psi)$ function from centrifuge experiments performed on soil samples. More recently, Peters and Durner (2006)

derived the objective function for the integral fit of centrifuge data. They also performed a sensitivity analysis of the error of the averaging method.

In contrast to soil physics, the point $\theta(\psi)$ function has been routinely extracted from centrifuge drainage experiments in petrophysics. Numerous techniques for interpreting effluent out-flow data obtained by steady-state centrifugation can be found in the petrophysics literature. Ruth and Chen (1995) and Forbes (1997) provided detailed reviews and comparative evaluations of the different computational procedures available. According to Christiansen (2001) these procedures can be divided into two main groups: differential and integral methods. Hassler and Brunner (1945) were the first to propose a method to calculate the point $\theta(\psi)$ function by differentiating the product of $<\theta>$ and the point ψ. They adopted a graphical approach to determining the gradient. Numerical differentiation or fitting a differentiable equation to the observation data can also be used (Christiansen, 2001). The alternative integral method uses a parametric expression for the point $\theta(\psi)$ function to predict θ from known values of ψ at discrete points along the length of the sample. The resulting θ values are numerically integrated to give the $<\theta>$ for a given angular velocity (ω). The calculated $<\theta>$ values are then compared to the measured $<\theta>$ values and, using an iterative least-square minimization technique, the parameters of the point equation are optimized. This one-dimensional integral method was originally described by Bentsen and Anli (1977). It is particularly versatile and attractive since it allows for the incorporation of any parametric expression for the point $\theta(\psi)$ function (Christiansen, 2001). Although discussed in Peters and Durner (2006, Appendix A), this method does not appear to have been previously applied in a soil physics context. Henceforth it will be referred to as the *integral method*.

The objectives of this paper are to: (i) introduce the integral method for determining the point $\theta(\psi)$ function with a centrifuge from the petrophysics literature to a soil physics audience, (ii) apply this method to extract point $\theta(\psi)$ functions for a range of porous media (Berea sandstone, glass beads, and Hanford sediments) using both the Brooks and Corey (1964) and van Genuchten (1980) equations, and (iii) compare the resulting point $\theta(\psi)$ functions with $<\theta>(<\psi>)$ functions for the same materials based on the averaging method of Reatto et al. (2008).

Materials and Methods

Sample Preparation

The following porous media were selected for study: Berea sandstone (a consolidated siliciclastic rock from Ohio widely employed as standard material in petroleum engineering), packed glass beads (a commonly used "ideal" porous medium in soil physics), and unconsolidated, coarse-textured sediments collected from four different locations at the Environmental Restoration Disposal Facility (ERDF) on the U.S. Department of Energy's (DOE) Hanford Reservation in the state of Washington. The Hanford sediments are of considerable environmental significance, and information about their point capillary pressure–saturation functions should be valuable for modeling the transport of transuranic waste in the Hanford vadose zone.

The Hanford samples consisted of both disturbed and undisturbed sediments. The disturbed sediments were the same as the fine- to medium-grained sand used in the flow and transport experiments reported by Pace et al. (2003) and Mayes et al. (2009) and referred to as HL (the same notation is used here). The other Hanford samples were all undisturbed cores excavated in August 2007 from an outcrop exposing three distinct sandy sedimentary layers (an upper coarse layer, UCL, a middle fine layer, MFL, and a lower coarse layer, LCL) at the ERDF. The undisturbed cores were obtained by first sculpting approximately cylindrical exposures of moist sediment, slightly larger than the desired sample dimensions. A cylindrical Delrin

sample holder (3.31 cm diameter, 5.78 cm length) was then gently pushed over each sculpted exposure resulting in a tight fit with minimal disturbance. The undisturbed cores were then temporarily sealed with impermeable caps. In the laboratory these caps were replaced with permeable Delrin discs, perforated with 0.5 mm holes. Cheesecloth was placed between the sample and the bottom disc to prevent migration of fine-grained particles through the disc perforations during centrifugation.

The spherical soda lime glass beads (manufactured under the name Dragonite® by Jaygo Inc., Union, NJ) were 45-70 μm in diameter, abbreviated as GB. The GB and HL samples were manually packed into the same Delrin sample holders that were used for collecting the undisturbed Hanford sediments. To minimize sample heterogeneity, both materials were moistened with de-aired water and added to the sample holders in ~5 mm layers. Each layer was tamped down with a glass rod and consolidated by tapping several times lightly on the sample holder. This process was repeated until each sample holder was full. The Berea sandstone samples were cylindrical rock cores (3.80 cm diameter, 4.78 cm length) supplied by Coretest Systems, Morgan Hill, CA, and did not require a sample holder. They were sleeved with Teflon tape to prevent flow of water along the side of the core. Three replicate samples of each of these six materials (i.e. 18 cores) were selected for study.

All the samples were flushed with CO_2 for 0.5 h, saturated from the base with de-aired water for 12 h, and placed under a partial vacuum for 3 h while immersed in water. The relative saturations, $S \equiv \theta/\phi$, achieved by this method were ≥ 95%. The unconsolidated samples were precompacted by centrifugation at an angular velocity of 1047 rad sec^{-1} (10,000 rpm) for 3 h to minimize any rearrangement of particles during the capillary pressure–saturation measurements. These samples were then resaturated following the same protocol as before. Next, the saturated hydraulic conductivity, K_{sat}, was determined with a constant head permeameter following procedures similar to those presented in Reynolds and Elrick (2002). The combined resistance to flow of elements of the sample holder assembly (perforated plates, cheese cloth, tubes, etc.) was determined in separate experiments and its effect on the

measured K_{sat} of the porous media was discounted. Dry bulk and particle densities were measured using gravimetry and pycnometry respectively, and then used to calculate the total porosity, ϕ (Flint and Flint, 2002). Particle-size distributions were determined by combining hydrometer measurements with sieve analyses following the procedures outlined in Gee and Or (2002). The physical properties of the samples are summarized in Table 1.

Centrifugation

The saturated pre-compacted samples were centrifuged with a URC-628 Ultra-Rock Core centrifuge (Coretest Systems, Morgan Hill, CA) described in detail by van den Berg et al. (2009). Each sample was subjected to several intervals of constant angular velocity, ω, centrifugation (Table 2). The ω values and their respective durations were selected based on drainage data from previous centrifuge experiments performed on extra samples of each material. For angular velocities <78.54 rad sec^{-1} (750 rpm) a stabilizing arm was used to prevent excessive rotor wobble. For higher angular velocities, the rotor was stopped to remove this stabilizing arm and restarted within 5 min. The effect of this stoppage time on the fluid distributions was assumed to be minimal (Baldwin and Yamanashi, 1989).

The centrifuge rotor holds three samples fitted with effluent collection cups. During operation the centrifuge automatically monitors the location of the air-water interface within each effluent collection cup. A dedicated data acquisition system converts the movement of this interface into a water volume time series for each sample (van den Berg et al., 2009). These data were exported and used to compute the total volumes of water produced at equilibrium for each constant ω interval. The outflow data were then post-processed to correct for drainage from the perforated plates and cheese cloth during centrifugation. A second post-processing correction was applied to account for any discrepancy between the total water production measured with the centrifuge and that obtained by weighing the samples before and after centrifugation.

Data Analysis

The average relative saturation, <S>, associated with a given ω, was calculated using:

$$< S > = \frac{PV - Q_w(\omega)}{PV} \qquad [1]$$

where $Q_w(\omega)$ is the cumulative volume of water (ml) produced by that ω value, and PV is the total pore volume of the sample (ml). The corresponding capillary pressure, ψ (Pa), at any point of interest along the radial through the center of the sample is given by Christiansen (2001):

$$\psi = \frac{1}{2}\Delta\rho\omega^2(r_o^2 - r^2) \qquad [2]$$

where Δρ is the density difference between the wetting and non-wetting fluids (kg m^{-3}), ω is the angular velocity (s^{-1}), r is the radial distance to any point on the axis of rotation of the cylindrical sample (m), and r_o is the radial distance to the effluent outlet (m). The average capillary pressure, <ψ> (Pa), for a sample subjected to a given ω was calculated from (Reatto et al., 2008):

$$< \psi >= \frac{k}{6}\frac{\omega^2 L}{g}(L - 3r_o) \qquad [3]$$

where g is the acceleration due to gravity (9.81 m s^{-2}), k is a conversion factor equal to 9807 Pa m^{-1}, and L is the length of the sample (m).

The centrifuge data were parameterized using the "constrained" form of the van Genuchten (1980) equation:

$$S = (1 - S)[1 + (\alpha|\psi|)^n]^{-\left(1-\frac{1}{n}\right)} + S_r \qquad [4]$$

where S_r is residual saturation (dimensionless), and α (Pa^{-1}) and n are empirical parameters. For the averaging method, S and ψ in Equation [4] were replaced with <S> and <ψ> from Equation [1] and [3], respectively. Gauss-Newton non-linear regression (SAS/STAT software, version 9.1.3, SAS Institute Inc. Cary, NC) was then used to estimate the S_r, α, and n parameters in Equation [4]. Point estimates of the same parameters were obtained using the integral method. Because detailed descriptions of the implementation of this method can be found in Schroth et al. (1996) for hanging water column or pressure cell experiments and in Bentsen and Anli (1977), Christiansen (2001) and Peters and Durner (2006) for centrifuge experiments, only an overview is provided here. Based on Equation [2], the average relative saturation can be written in the following form:

$$< S > (\omega) = \frac{1}{r_o - r_i} \int_{r_i}^{r_o} S[\psi(r, \omega)] dr \qquad [5]$$

where r_i is the radial distance to the air inlet (m). Because ψ is known for any location along the sample from Equation [2] (we used r = r_i), best estimates of the van Genuchten parameters can be obtained by substituting Equation [4] into Equation [5] and minimizing the difference between the calculated and observed average saturations. Because point-based capillary pressure-saturation data are more likely to exhibit a distinct air-entry value, the Brooks and Corey (1964) equation may be more applicable than the van Genuchten (1980) equation when using the integral method. The Brooks and Corey equation (1964) can be written as:

$$S = (1 - S_r)\left(\frac{\psi_a}{\psi}\right)^{\lambda} + S_r \quad \{\psi > \psi_a\} \qquad [6a]$$

$$S = 1 \qquad \{\psi \leq \psi_a\} \qquad [6b]$$

where ψ_a is the air entry value (kg m^2 s^{-2}), and λ is the pore-size distribution index. Equation [6] was substituted into Equation [5], and values of the S_r, ψ_a, and λ parameters were adjusted iteratively until the difference between the calculated and observed average saturations was reduced to a minimum. All of the integral method optimizations were performed using the Microsoft Excel® spreadsheet program PcCentData from Christiansen (2001), which was modified to accommodate the van Genuchten (1980) and Brooks and Corey (1964) equations.

Results and Discussion

Quasi steady-state centrifuge experiments were performed on 18 samples as described above. Water production during centrifugation showed rapid adaptation to each stepwise increase in angular velocity followed by longer periods in which little water was produced as the hydraulic gradients approached equilibrium (Figure 1). Outflow at high angular velocities (i.e., $\omega > 523.6$ s^{-1}) was always very small as compared with the amounts obtained in the preceding intervals. Estimates of saturation were based on the total volumes of water produced during each constant ω interval, and assumed that hydraulic equilibrium was reached prior to increasing ω.

Application of the van Genuchten (1980) equation to the <S> versus <ψ> data pairs obtained using the averaging method produced the suite of parameter estimates given in Table 3. Goodness of fit, as quantified by the RMSE, was generally very good with a mean value of 1.52×10^{-2} and a maximum value of 2.43×10^{-2}. An example fit of the van Genuchten (1980) equation to the averaging method data is shown in Figure 2.

In the integral method, the modeled <S> values were matched to the measured <S> values by iteratively adjusting the parameters of the van Genuchten (1980) equation using PcCentData (Christiansen, 2001). Figure 3 shows that a very good correspondence was achieved between the measured and modeled average relative saturations (denoted by the closed and open circles, respectively). The point-based

function that gave the best fit between the measured and modeled <S> values is represented by the line in Figure 3. It is important to stress that this function was obtained by optimizing Equation [4] to the experimental data, hence the discrepancy between the line and the circles in Figure 3. This is to be expected because the use of <S> values smoothes out the drainage curve. As a result, the van Genuchten (1980) function for a physical point (the line in Figure 3) is much steeper than the corresponding function obtained by simply fitting the <S> values (the line in Figure 2).

The mean and maximum RMSE values resulting from the point-based van Genuchten (1980) equation fits were 1.29×10^{-2} and 2.06×10^{-2}, respectively (Table 4). A paired t-test indicated that the RMSE value from the integral method was significantly lower than the mean value from the averaging method at the 95% confidence level. Thus, not only does the integral method provide a more accurate physical description of the drainage process than the averaging method, but it also provides a better fit to the experimental data.

Best fit estimates of the point-based van Genuchten (1980) equation parameters are summarized in Table 4. To facilitate comparison with the corresponding parameters from the averaging method, 1:1 plots were constructed for S_r, α, and n (Figs. 4-6). Estimates of the residual water content varied between 0.097 and 0.283 for the averaging method and between 0.093 and 0.273 for the integral method (Tables 3 and 4). There was a slight trend towards over estimation of S_r by the averaging method, but in general both sets of parameter estimates were very close to each other (Figure 4). This is because the average relative saturation is quite similar to the point relative saturation at r_i for the high capillary pressures produced by high angular velocities (Figure 3).

Estimates of α varied between 0.087 and 1.467 kPa^{-1} for the averaging method and between 0.076 and 1.389 kPa^{-1} for the integral method (Tables 3 and 4). For low values of α (less than $\sim$0.3 kPa^{-1}) both methods yielded similar estimates of this parameter (Figure 5). The averaging method consistently overestimated the larger α

values, however, compared with the integral method. The α parameter in Equation [4] determines the location of the air-entry region on the capillary pressure-saturation curve. Thus, any overestimation of α will lead to a shift in the air entry region towards lower suctions, with a corresponding overprediction of the diameter of the largest pores present. This effect was most pronounced for the coarse-textured UCL and LCL samples from Hanford.

Estimates of the dimensionless n parameter varied between 1.658 and 3.191 for the averaging method and between 1.913 and 9.523 for the integral method (Tables 3 and 4). Unlike the other two fitted parameters in Equation [4], the n parameter showed a major curvilinear deviation from the 1:1 line for the two estimation methods (Figure 6). The n parameter controls the steepness of the capillary pressure-saturation function as water drains at suctions > $1/\alpha$; the larger the value of n, the steeper the curve. It is clear from Figure 6 that the averaging method systematically underestimated this parameter relative to the point-based estimates. Any underestimation of n will lead to an over prediction of the breadth of the pore-size distribution. The source of this bias is the averaging method's reliance on the <S> and <ψ> values, which in effect smoothes out measurements of the drainage process. The magnitude of the error introduced by this smoothing process will be greatest for coarse-textured materials in long sample columns (Dane and Hopmans, 2002c).

The Brooks and Corey (1964) function, Equation [6], may be more applicable to point-based data than the van Genuchten (1980) function, Equation [4]. This is because Equation [6] is a segmented model that contains a distinct air entry value, ψ_a, separating the saturated portion of the capillary pressure-saturation curve from the partially-drained region. Theoretically, a sharp break is to be expected at a physical point, whereas an air entry region, as represented by the α parameter in the van Genuchten (1980) equation, best describes the drainage process when it is averaged over a finite volume. To explore possible modeling variations between the Brooks and Corey (1964) and van Genuchten (1980) functions, the integral method was also

implemented using Equation [6] instead of Equation [4] for comparison with the preceding results. The goodness of fit and parameter estimates are summarized in Table 5, with a typical result shown in Figure 7. The mean and maximum RMSS values for Equation [6] were 1.30×10^{-2} and 2.11×10^{-2}, respectively (Table 5). A paired t-test indicated no significant difference (at the 95% confidence level) between the mean RMSS values for Equation [4] and [6] fitted to the integral method data for a physical point. We anticipated a better fit for Equation [6] than for Equation [4] for the reasons described above. The absence of any difference between the two models may be related to the limited number of data pairs in the low suction range.

Figure 8 compares the capillary pressure-saturation functions for the Berea-1 sample resulting from the three modeling approaches (averaging method with Equation [4], integral method with Equation [4], and integral method with Equation [6]). The functions are clearly sensitive to the different modeling methods. Regardless of the equation used, the two point–based functions are similar at intermediate and high $|\psi|$ values, predicting more rapid drainage and lower saturations than the averaging method function. In contrast, at low $|\psi|$ values, the two van Genuchten (1980) functions (for the averaging and integral methods) are quite similar, while the point-based Brooks and Corey (1964) function exhibits a sharp break in slope at the air entry value and higher relative saturation values.

Maximum deviations between the relative saturations predicted by the averaging and integral methods ranged from 0.078 to 0.281 (Table 6). The largest deviations were for the glass bead (GB) samples, which had the narrowest range of pore sizes. The smallest deviations were for the Berea sandstone samples, which had a relatively broad range of pore sizes. The point-based Brooks and Corey (1964) model produced higher maximum deviations than the point-based van Genuchten (1980) model in 14 out of the 18 samples investigated (Table 6). With the sole exception of the Berea cores, these maximum deviations occurred at $|\psi|$ values <10 kPa. For all of the samples, the maximum deviations observed for the Brooks and Corey (1964) equation occurred at suctions less than or equal to those at which the

maximum deviations occurred for the van Genuchten (1980) equation. These trends can be attributed to the more precise representation of air entry at a physical point by the Brooks and Corey (1964) function.

Based on the above results we recommend use of the integral method instead of the averaging method for determining the capillary pressure-saturation function using steady-state centrifugation. Use of the averaging method results in a smoothing out of the drainage process, which can lead to inaccurate predictions of other hydraulic properties such as the relative permeability function. The integral method clearly improves data evaluation and can be implemented with any parametric model. We used the "constrained" van Genuchten (1980) and Brooks and Corey (1964) models, which gave similar results, although the later provides a more physically precise description of air entry at a physical point.

Reatto et al. (2008) report an approximate one-to-one relationship between capillary pressure-saturation curves determined by steady-state centrifugation and those measured using the pressure plate method. Other authors, however, have noted significant deviations between data sets obtained with these two methods (e.g., Omoregie, 1988; Khanzode et al., 2002). We suggest the "good correspondence" observed by Reatto et al. (2008) was mainly due to the short column length used (5 cm) and the fine texture of most of their samples (average clay content of 469 g kg^{-1}). It may also be somewhat fortuitous due to the following confounding factors. First, their comparison was between centrifuged and non-centrifuged samples, and centrifugation is known to produce changes in total porosity and pore-size distribution relative to undisturbed material (Nimmo and Akstin, 1988). The effects of such changes on the capillary pressure-saturation function are well documented (Stange and Horn, 2005 and Assouline, 2006). No mention is made of this important issue in the paper by Reatto et al (2008). Second, their comparison was between centrifuge $<\theta>(<\psi>)$ curves and pressure plate $<\theta>(\psi)$ curves. A more meaningful comparison would have been between the point $\theta(\psi)$ curves extracted from these two methods. Such a comparison is needed to document the effects of any centrifuge-

induced compaction on soil water retention. In our opinion, the steady-state centrifuge method requires further investigation before it can be recommended for the routine measurement of capillary pressure-saturation curves on unconsolidated materials.

References

Assouline, S. 2006. Modeling the relationship between soil bulk density and the water retention curve. Vadose Zone J. 5:554–563.

Baldwin, B.A., and W.S. Yamanashi. 1989. Persistence of nonuniform brine saturation distribution in SCA electrical resistivity study core plugs after desaturation by centrifuging. Log Anal. 30:45–48.

Bentsen, R.G., and J. Anli. 1977. Using parameter estimation techniques to convert centrifuge data into a capillary–pressure curve. SPE J. 17:57–64.

Briggs, L.J., and J.W. McLane. 1907. The moisture equivalents of soils. USDA Bur. of Soils Bull. 45. U.S. Gov. Print. Office, Washington, DC.

Brooks, R.H., and A.T. Corey. 1964. Hydraulic properties of porous media. Hydrol. Pap. 3. Colorado State Univ., Fort Collins.

Christiansen, R.L. 2001. Two-phase flow through porous media. Colorado School of Mines, Boulder.

Dane, J.H., and J.W. Hopmans. 2002a. Hanging water column. p. 680–683. In J.H. Dane and G.C. Topp (ed.). Methods of soil analysis. Part 4. Physical methods. SSSA Book Ser. 5. SSSA, Madison, WI.

Dane, J.H., and J.W. Hopmans. 2002b. Pressure plate extractor. p. 688–690. In J.H. Dane and G.C. Topp (ed.). Methods of soil analysis. Part 4. Physical methods. SSSA Book Ser. 5. SSSA, Madison, WI.

Dane, J.H., and J.W. Hopmans. 2002c. Computational corrections. p. 714–717. In J.H. Dane and G.C. Topp (ed.). Methods of soil analysis. Part 4. Physical methods. SSSA Book Ser. 5. SSSA, Madison, WI.

Dane, J.H., M. Oostrom, and B.C. Missildine. 1992. An improved method for the determination of capillary pressure–saturation curves involving TCE, water and air. J. Contam. Hydrol. 11:69–81.

Flint, A.L., and L.E. Flint. 2002. Total porosity. p. 242–245. In J.H. Dane and G.C. Topp (ed.). Methods of soil analysis. Part 4. Physical methods. SSSA Book Ser. 5. SSSA, Madison, WI.

Forbes, P.L. 1997. Centrifuge data analysis techniques: An SCA survey on the calculation of drainage capillary pressure curves from centrifuge measurements. SCA-9714. In Int. Symp. Soc. Core Anal., Calgary, AB, Canada. 8–10 Sept. 1997. Soc. Core Anal., Dublin, CA.

Gardner, R.A. 1937. A method of measuring the capillary tension of soil moisture over a wide moisture range. Soil Sci. 43:277–283.

Gee, G.W., and D. Or. 2002. Particle-size analysis. p. 255–289. In J.H. Dane and G.C. Topp (ed.). Methods of soil analysis. Part 4. Physical methods. SSSA Book Ser. 5. SSSA, Madison, WI.

Hassler, G.L., and E. Brunner. 1945. Measurement of capillary pressures in small core samples. Trans. Am. Inst. Min. Metall. Pet. Eng. 160:114–123.

Jalbert, M., and J.H. Dane. 2001. Correcting laboratory retention curves for hydrostatic fluid distributions. Soil Sci. Soc. Am. J. 65:648–654.

Jalbert, M., J.H. Dane, and J.H. Liu. 1999. TrueCell: Physical point Brooks–Corey parameters using pressure cell data. Users guide for version 1.2. Spec. Rep. Dep. of Agron. and Soils, Auburn Univ., Auburn, AL.

Khanzode, R.M., S.K. Vanapalli, and D.G. Fredlund. 2002. Measurement of soil-water characteristic curves for fi ne-grained soils using a small-scale centrifuge. Can. Geotech. J. 39:1209–1217.

Liu, H.H., and J.H. Dane. 1995a. Improved computational procedure for retention relations of immiscible fluids using pressure cells. Soil Sci. Soc. Am. J. 59:1520–1524.

Liu, H.H., and J.H. Dane. 1995b. Computation of the Brooks–Corey parameters at a physical point based on pressure cell data. Spec. Rep. Dep. of Agron. and Soils, Auburn Univ., Auburn, AL.

Mayes, M.A., G. Tang, P.M. Jardine, L.D. McKay, X.L. Yin, M.N. Pace, J.C. Parker, F. Zhang, T.L. Mehlhorn, and R.N. Dansby-Sparks. 2009. Influence of sedimentary bedding on reactive transport parameters under unsaturated condition. Soil Sci. Soc. Am. J. 73:1938–1946.

Nimmo, J.R., and K.C. Akstin. 1988. Hydraulic conductivity of a sandy soil at low water content after compaction by various methods. Soil Sci. Soc. Am. J. 52:303–310.

Odén, S. 1975. An integral method for the determination of moisture retention curves by centrifugation. Grundfoerbaettring 27:137–143.

Omoregie, Z.S. 1988. Factors affecting the equivalency of different capillary pressure measurement techniques. SPE Form. Eval. 3(1):147–155.

Pace, M.N., M.A. Mayes, P.M. Jardine, T.L. Mehlhorn, J.M. Zachara, and B.N. Bjornstad. 2003. Quantifying the effects of small-scale heterogeneities on flow and transport in undisturbed cores from the Hanford formation. Vadose Zone J. 2:664–676.

Perfect, E., L.D. McKay, S.C. Cropper, S.G. Driese, G. Kammerer, and J.H. Dane. 2004. Capillary pressure–saturation relations for saprolite: Scaling with and without correction for column height. Vadose Zone J. 3:493–501.

Peters, A., and W. Durner. 2006. Improved estimation of soil water retention characteristics from hydrostatic column experiments. Water Resour. Res. 42:W11401, doi:10.1029/2006WR004952.

Reatto, A., E.M. da Silva, A. Bruand, E.S. Martins, and J.E.F.W. Lima. 2008. Validity of the centrifuge method for determining the water retention properties of tropical soils. Soil Sci. Soc. Am. J. 72:1547–1553.

Reynolds, W.D., and D.E. Elrick. 2002. Constant head soil core (tank) method. p. 804–808. In J.H. Dane and G.C. Topp (ed.). Methods of soil analysis. Part 4. Physical methods. SSSA Book Ser. 5. SSSA, Madison, WI.

Russell, M.B., and L.A. Richards. 1938. The determination of soil moisture energy relations by centrifugation. Soil Sci. Soc. Am. Proc. 3:65–69.

Ruth, D.W., and Z.A. Chen. 1995. Measurement and interpretation of centrifuge capillary pressure data: The SCA survey data. Log Anal. 36:21–33.

Sakaki, T., and T.H. Illangasekare. 2007. Comparison of height-averaged and point measured capillary pressure–saturation relations for sands using a modified Tempe cell. Water Resour. Res. 43:W12502, doi:10.1029/2006WR005814.

Schroth, M.H., S.J. Ahearn, J.S. Selker, and J.D. Istok. 1996. Characterization of Miller-similar silica sands for laboratory hydrologic studies. Soil Sci. Soc. Am. J. 60:1331–1339.

Stange, C.F., and R. Horn. 2005. Modeling the soil water retention curve for conditions of variable porosity. Vadose Zone J. 4:602–613.

Tokunaga, T.K., J. Wan, and K.R. Olson. 2002. Saturation–matric potential relations in gravel. Water Resour. Res. 38(10):1214, doi:10.1029/2001WR001242.

van den Berg, E.H., E. Perfect, C. Tu, P.S.K. Knappet, T.P. Leao, and R.W. Donat. 2009. Unsaturated hydraulic conductivity measurements with centrifuges: A review. Vadose Zone J. 8:531–547.

van Genuchten, M.Th . 1980. A closed-form equation for predicting the hydraulic conductivity of unsaturated soils. Soil Sci. Soc. Am. J. 44:892–898.

Appendix II-A Tables

Table 1. Physical properties of median grain diameter (d50), porosity (ϕ), and saturated hydraulic conductivity (K_{sat}) for the Berea sandstone, glass beads (GB), and disturbed (HL) and undisturbed upper coarse layer (UCL), middle fine layer (MFL), and lower course layer (LCL) Hanford sediments investigated.

Sample-replicate no.	D50 (μm)	Φ ($m^3\ m^{-3}$)	K_{sat} ($m\ s^{-1}$)
Berea-1	NA†	0.183ǂ	9.48×10^{-6}ǂ
Berea-2	NA†	0.182ǂ	6.50×10^{-6}ǂ
Berea-3	NA†	0.188ǂ	1.28×10^{-6}ǂ
GB-1	58₴	0.367	6.26×10^{-5}
GB-2	58₴	0.362	6.75×10^{-5}
GB-3	58₴	0.360	6.83×10^{-5}
HL-1	98	0.413	5.34×10^{-5}
HL-2	98	0.415	3.43×10^{-5}
HL-3	98	0.411	4.18×10^{-5}
UCL-1	360	0.302	6.09×10^{-5}
UCL-2	400	0.346	1.46×10^{-4}
UCL-3	400	0.361	6.74×10^{-5}
MFL-1	310	0.322	1.64×10^{-4}
MFL-2	290	0.318	1.20×10^{-4}
MFL-3	290	0.321	1.81×10^{-4}
LCL-1	310	0.389	1.02×10^{-3}
LCL-2	410	0.396	4.32×10^{-4}
LCL-3	310	0.385	3.93×10^{-4}

† NA, not applicable for consolidated samples

ǂ Data supplied by Coretest Systems, Morgan Hill, CA.

₴ Calculated as mean of upper and lower size bounds for fraction.

Table 2. Number and duration (t) of constant angular velocity (ω) periods used in the centrifuge experiments with Berea sandstone, glass beads (GB), and disturbed (HL) and undisturbed upper course layer (UCL), middle fine layer (MFL), and lower coarse layer (LCL) Hanford sediments.

Constant	Berea		GB		HL		UCL		MFL		LCL	
ω period	ω s^{-1}	t h	ω s^{-1}	t h	ω s^{-1}	t h	ω s^{-1}	t h	ω s^{-1}	t h	ω s^{-1}	t h
1	51.4	5	36.7	12	49.7	12	41.9	6	49.7	6	41.9	6
2	78.5	5	41.9	12	57.6	12	49.7	6	57.6	6	49.7	6
3	104.7	5	49.7	12	62.8	12	57.6	6	78.5	6	57.6	6
4	130.9	4	57.6	12	73.3	12	68.1	6	104.7	6	68.1	6
5	157.1	7.5	62.8	12	83.8	12	83.8	6	209.4	6	83.8	6
6	209.4	7.5	73.3	12	94.2	12	104.7	6	418.9	6	104.7	6
7	314.2	7.5	83.8	12	104.7	12	209.4	6	628.3	3	209.4	3
8	418.8	7.5	94.2	12	130.9	12	418.9	6	942.5	3	733.0	3
9	523.6	10	104.7	12	157.1	12	628.3	6				
10	942.5	18	130.9	12	183.3	12	942.5	6				
11			157.1	12	209.4	12						
12			183.3	12	314.2	12						
13			209.4	12	523.6	12						
14			314.2	12	733.0	12						
15			523.6	12	942.5	12						
16			733.0	12								
17			942.5	21								

Table 3. Summary of van Genuchten (1980) model fits and estimates of the residual saturation, S_r, and α and n parameters for the averaging method of Reatto et al. (2008) for the Berea sandstone, glass beads (GB), and disturbed (HL) and undisturbed upper coarse layer (UCL), middle fine layer (MFL), and lower coarse layer (LCL) Hanford sediments.

Sample-replicate no.	S_r	α (kPa^{-1})	n	RMSE
Berea-1	0.178	0.087	1.893	2.36×10^{-2}
Berea-2	0.160	0.131	1.671	8.11×10^{-3}
Berea-3	0.143	0.119	1.658	6.29×10^{-3}
GB-1	0.203	0.123	3.191	2.43×10^{-2}
GB-2	0.176	0.115	2.942	1.96×10^{-2}
GB-3	0.214	0.116	3.086	1.94×10^{-2}
HL-1	0.255	0.160	2.531	1.88×10^{-2}
HL-2	0.277	0.161	2.544	2.00×10^{-2}
HL-3	0.245	0.161	2.537	1.95×10^{-2}
UCL-1	0.097	0.276	2.177	1.52×10^{-2}
UCL-2	0.127	0.638	2.139	8.28×10^{-3}
UCL-3	0.119	0.553	2.140	6.16×10^{-3}
MFL-1	0.283	0.237	2.268	1.81×10^{-2}
MFL-2	0.273	0.290	2.131	1.35×10^{-2}
MFL-3	0.265	0.258	2.191	1.13×10^{-2}
LCL-1	0.097	1.237	1.856	1.32×10^{-2}
LCL-2	0.151	1.467	1.755	1.52×10^{-2}
LCL-3	0.127	1.376	1.782	1.22×10^{-2}

Table 4. Summary of van Genuchten (1980) model fits and estimates of the residual saturation, S_r, and α and n parameters for the integral method of Bentsen and Anli (1977) for the Berea sandstone, glass beads (GB), and disturbed (HL) and undisturbed upper coarse layer (UCL), middle fine layer (MFL), and lower course layer (LCL) Hanford sediments.

Sample-replicate no.	S_r	α (kPa^{-1})	n	RMSE
Berea-1	0.184	0.076	2.442	2.06×10^{-2}
Berea-2	0.169	0.120	1.920	9.30×10^{-3}
Berea-3	0.155	0.108	1.913	7.27×10^{-3}
GB-1	0.169	0.108	9.523	9.39×10^{-3}
GB-2	0.147	0.103	5.867	2.01×10^{-2}
GB-3	0.183	0.103	7.220	1.16×10^{-2}
HL-1	0.239	0.141	4.337	1.49×10^{-2}
HL-2	0.262	0.142	4.471	1.51×10^{-2}
HL-3	0.228	0.143	4.335	1.64×10^{-2}
UCL-1	0.093	0.239	3.195	9.57×10^{-3}
UCL-2	0.126	0.482	3.877	5.71×10^{-3}
UCL-3	0.115	0.457	3.269	7.95×10^{-3}
MFL-1	0.278	0.206	3.489	1.74×10^{-2}
MFL-2	0.269	0.249	3.107	1.36×10^{-2}
MFL-3	0.261	0.222	3.291	1.03×10^{-2}
LCL-1	0.100	1.062	2.354	1.38×10^{-2}
LCL-2	0.154	1.389	2.040	1.59×10^{-2}
LCL-3	0.129	1.272	2.109	1.29×10^{-2}

Table 5. Summary of Brooks and Corey (1964) model fits and estimates of the residual saturation S_r, air-entry value ψa, and pore-size distribution index λ for the integral method of Bentsen and Anli (1977) for the Berea sandstone, glass beads (GB), and disturbed (HL) and undisturbed upper coarse layer (UCL), middle fine layer (MFL), and lower coarse layer (LCL) Hanford sediments.

Sample-replicate no.	S_r	ψ_a (kPa)	λ	RMSE
Berea-1	0.152	7.298	0.827	1.29×10^{-2}
Berea-2	0.128	4.319	0.573	1.38×10^{-2}
Berea-3	0.137	9.700	0.694	1.36×10^{-2}
GB-1	0.168	7.695	4.798	1.10×10^{-2}
GB-2	0.145	7.354	2.881	2.10×10^{-2}
GB-3	0.181	7.663	3.515	1.28×10^{-2}
HL-1	0.235	5.021	2.066	1.33×10^{-2}
HL-2	0.258	5.057	2.134	1.32×10^{-2}
HL-3	0.225	4.995	2.086	1.49×10^{-2}
UCL-1	0.086	2.736	1.401	9.12×10^{-3}
UCL-2	0.125	1.650	2.384	5.24×10^{-3}
UCL-3	0.115	1.679	1.883	9.18×10^{-3}
MFL-1	0.277	3.467	1.781	1.78×10^{-2}
MFL-2	0.267	2.831	1.554	1.44×10^{-2}
MFL-3	0.259	3.183	1.655	1.10×10^{-2}
LCL-1	0.099	0.736	1.216	1.33×10^{-2}
LCL-2	0.154	0.569	0.954	1.53×10^{-2}
LCL-3	0.129	0.617	1.012	1.24×10^{-2}

Table 6. Maximum deviations in relative saturation (ΔS) between the averaging and integral methods for the Brooks-Corey (BC) or van Genuchten (VG) models for the Berea sandstone, glass beads (GB), and disturbed (HL) and undisturbed upper coarse layer (UCL), middle fine layer (MFL), and lower coarse layer (LCL) Hanford sediments.

Sample-replicate no.	Max. |ΔSBC|	Max. |ΔSVG|
Berea-1	0.078	0.098
Berea-2	0.083	0.063
Berea-3	0.083	0.066
GB-1	0.281	0.228
GB-2	0.258	0.224
GB-3	0.244	0.216
HL-1	0.177	0.139
HL-2	0.177	0.130
HL-3	0.171	0.140
UCL-1	0.129	0.137
UCL-2	0.164	0.145
UCL-3	0.158	0.133
MFL-1	0.156	0.127
MFL-2	0.130	0.114
MFL-3	0.127	0.110
LCL-1	0.133	0.107
LCL-2	0.115	0.096
LCL-3	0.115	0.093

Appendix II-A Figures

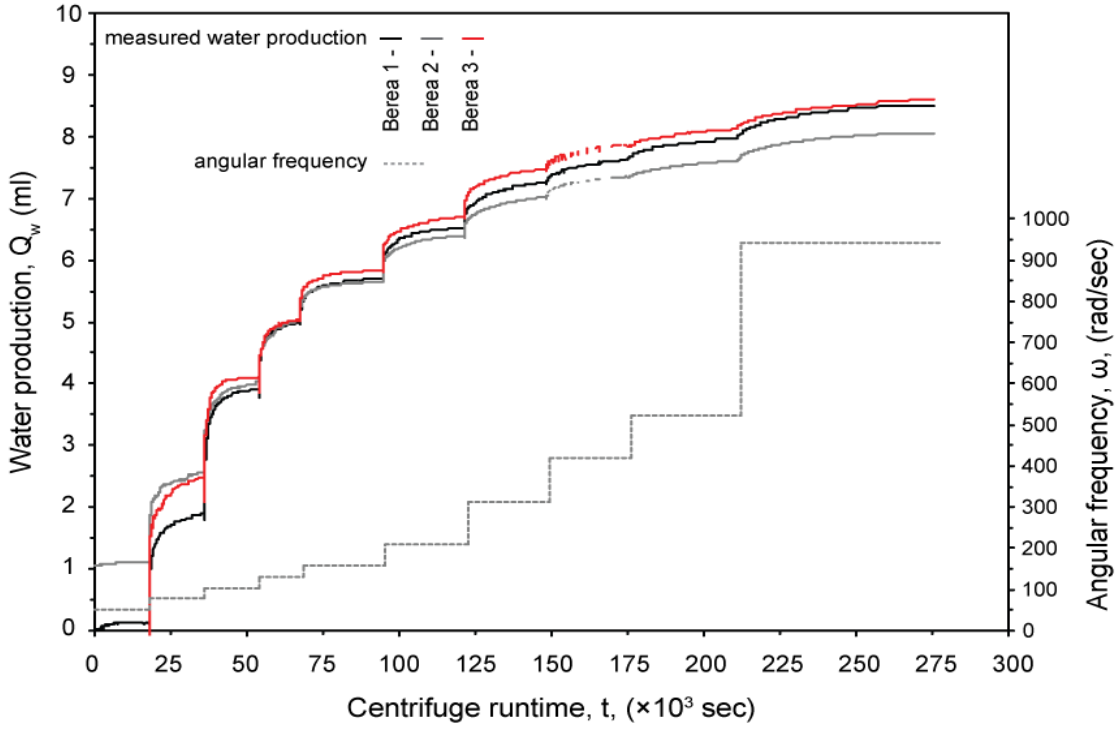


Figure 1. Step changes in centrifuge angular velocity, ω (lower curve), and corresponding water outflow, Q_w (upper curves), through time for the three replicate samples of Berea sandstone.

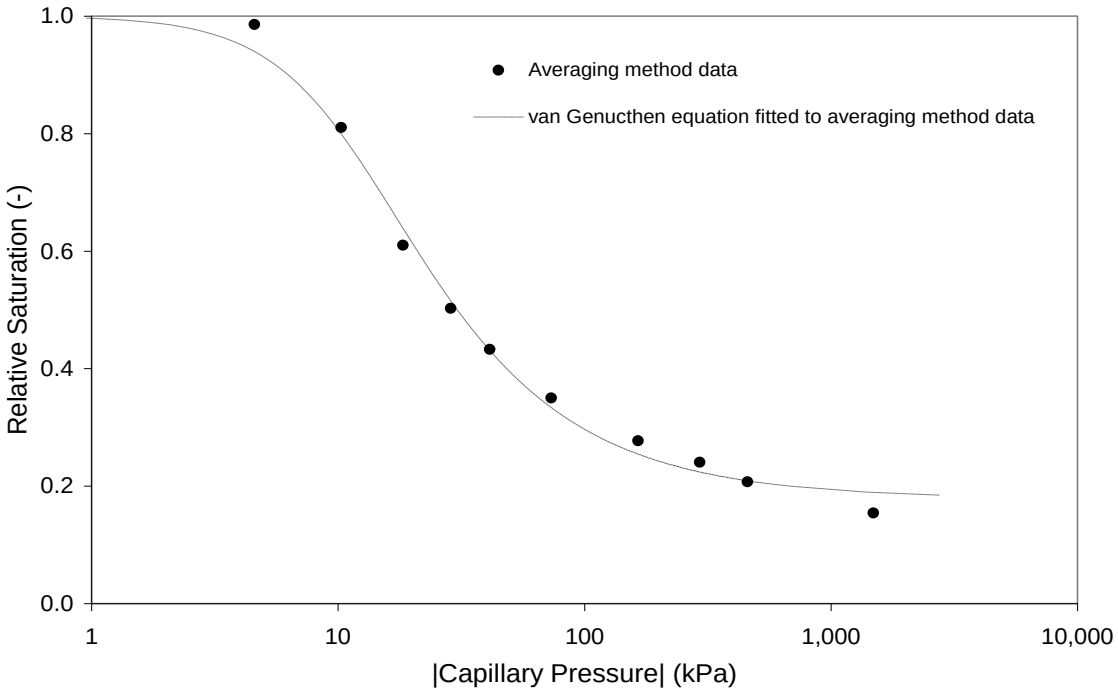


Figure 2. Measured capillary pressure-saturation data and fitted van Genuchten (1980) function for the Berea-1 sandstone sample based on the averaging method of Reatto et al. (2008).

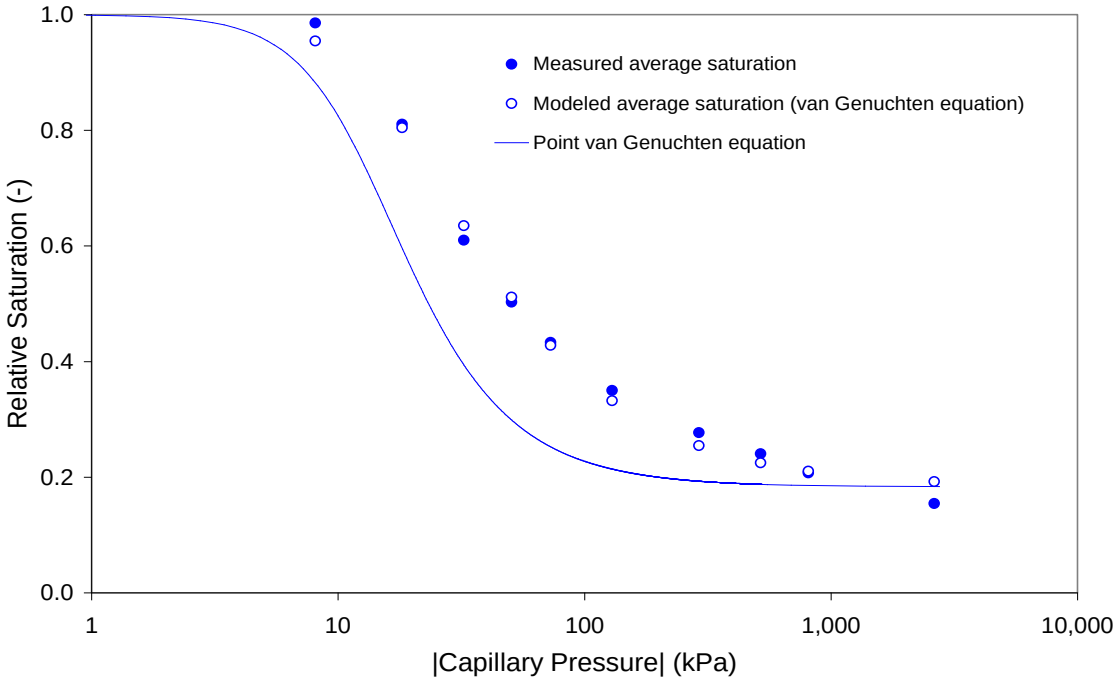


Figure 3. Measured and modeled average saturations and resulting point van Genuchten (1980) capillary pressure-saturation function for the Berea-1 sandstone sample based on the integral method of Bentsen and Anli (1977).

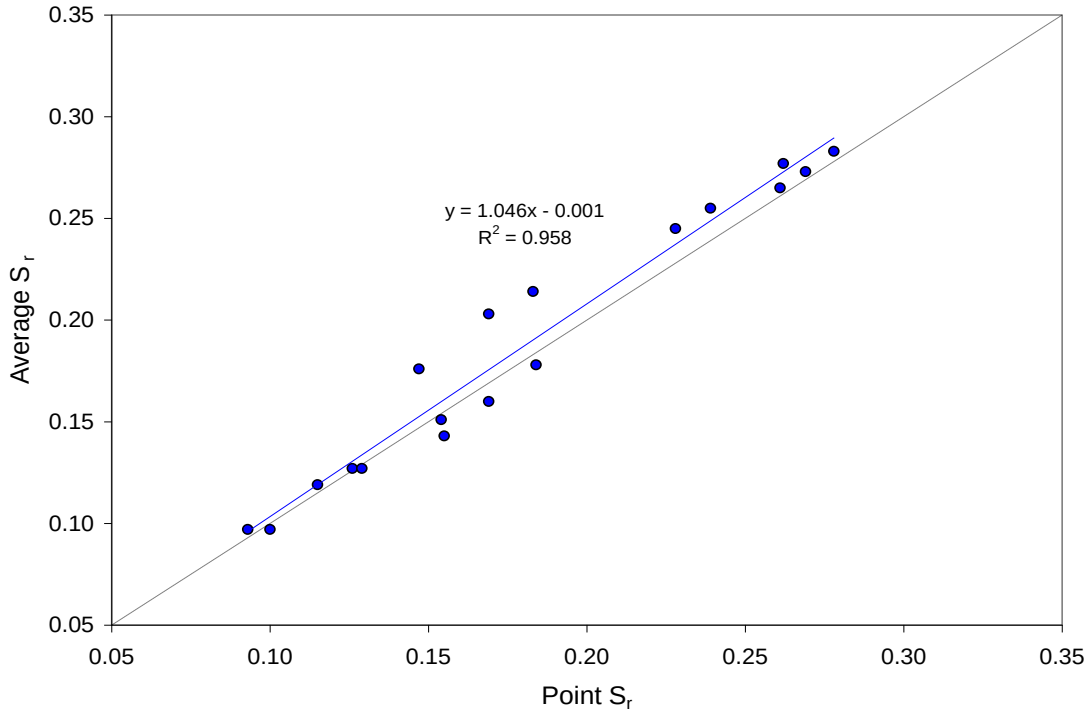


Figure 4. Relationship between residual saturation (S_r) values in the van Genuchten (1980) capillary pressure-saturation equation estimated using the averaging and integral methods. The dashed line indicates a 1:1 correspondence.

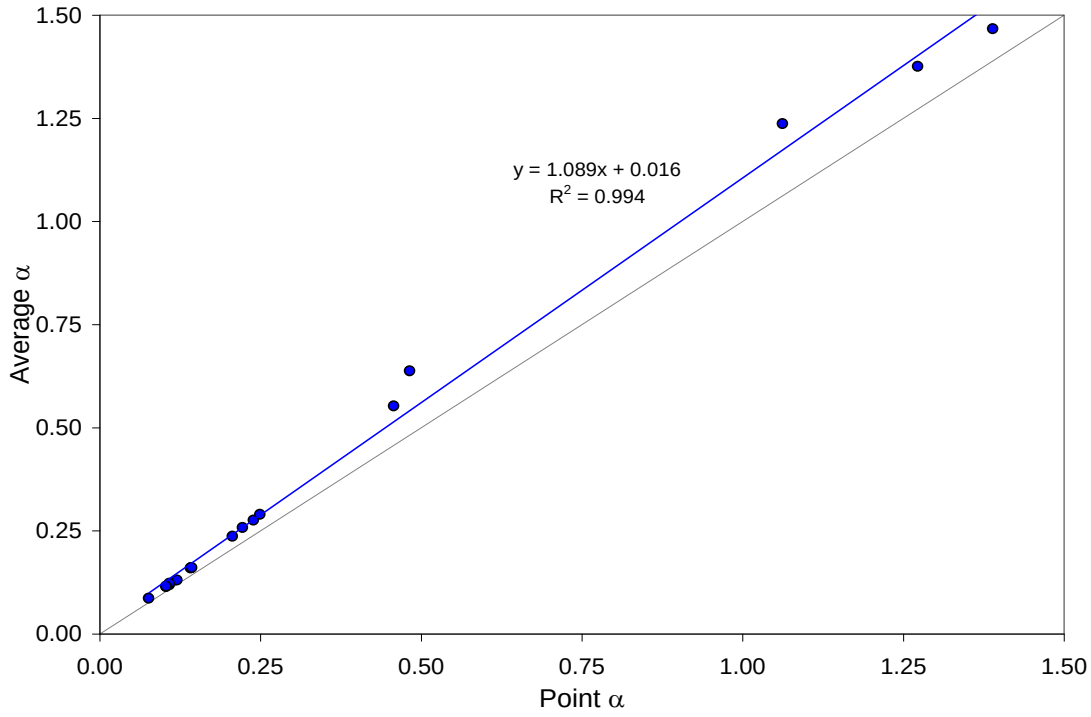


Figure 5. Relationship between the α parameter in the van Genuchten (1980) capillary pressure-saturation equation estimated using the averaging and integral methods. The dashed line indicates a 1:1 correspondence.

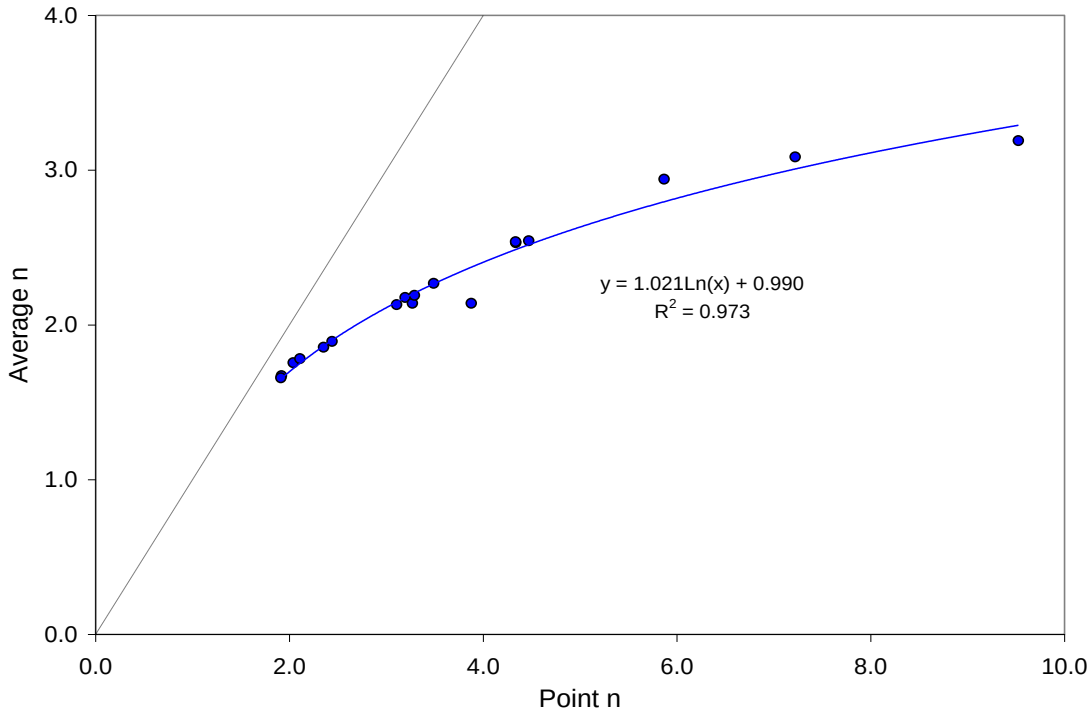


Figure 6. Relationship between the n parameter in the van Genuchten (1980) capillary pressure-saturation equation estimated using the averaging and integral methods. The dashed line indicates a 1:1 correspondence.

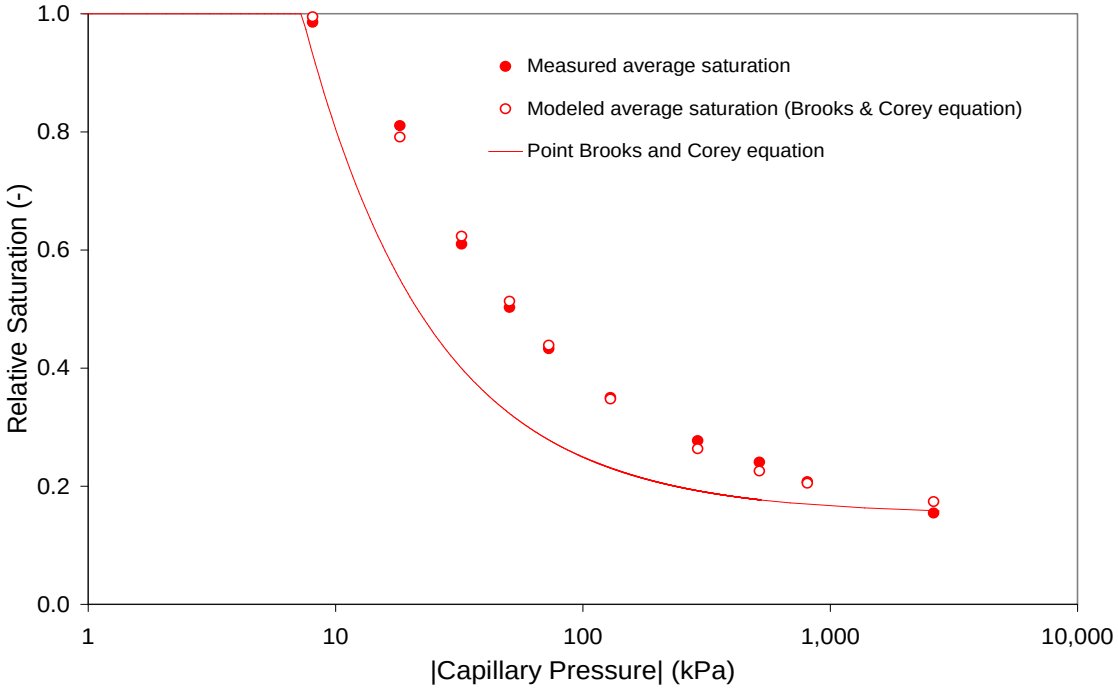


Figure 7. Measured and modeled average saturations and resulting point Brooks and Corey (1964) capillary pressure-saturation function for the Berea-1 sandstone sample based on the integral method of Bentsen and Anli (1977).

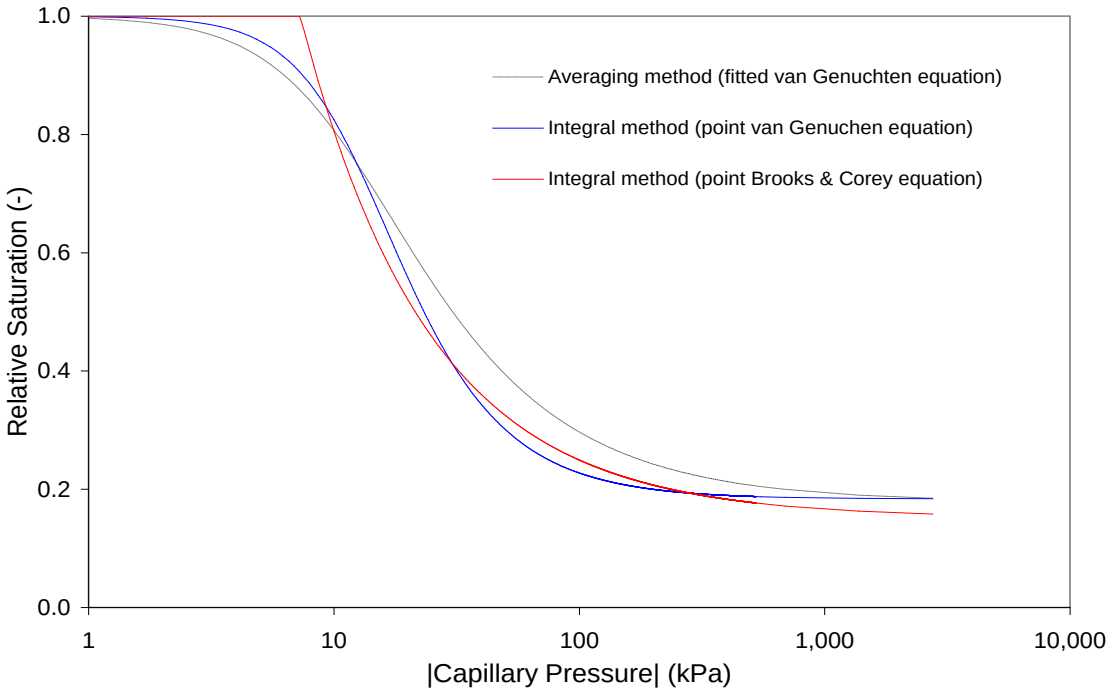


Figure 8. Comparison of capillary pressure-saturation function for the Berea-1 sample obtained using the averaging and integral methods.

Chapter III

Modeling the Impact of Capillary Pressure – Saturation Parameters on Geologic Carbon Sequestration Simulations

This chapter has not previously been published, nor will it be before the final version of this dissertation is submitted.

Samuel Clark Cropper contributed to this chapter by performing the data analysis and writing the paper. Others contributed by revising the manuscript.

Abstract

STOMP (Subsurface Transport Over Multiple Phases) is a numerical modeling tool that can be used to model CO_2 injection into deep saline aquifers for geologic carbon sequestration. Properties of the aquifer including porosity, intrinsic permeability, and capillary pressure – saturation parameters are required to create accurate simulations of CO_2 flow into the target aquifer. Use of the average capillary pressure-average saturation function, $<\theta>(\psi)$, instead of the point capillary pressure-saturation function, $\theta(\psi)$ in flow and transport models can produce erroneous predictions of important hydraulic properties. The purpose of this paper is to compare STOMP simulations in Berea sandstone cores using point capillary pressure-saturation function, $\theta(\psi)$, parameters to simulations using average capillary pressure-saturation function, $<\theta>(\psi)$, parameters to observe the effect on CO_2 injection flow rates and cost of injection. Results show simulations based on point parameters have injection flow rates 1.36 times the injection flow rates produced by simulations based on the average parameter set. An analysis of injection cost efficiencies show that simulations based on the point parameters reduce cost of injections significantly over average parameters sets. For example, the cost per ton of CO_2 injected at a mean gas pressure of 1.5×10^7 Pa was \$0.87 using the average parameter set and \$0.65 using the point parameter set.

Introduction

Increasing levels of anthropogenic CO_2 in the atmosphere over the past several decades have led to increased interest in methods to remove CO_2 from the atmosphere. Geologic Carbon Sequestration (GCS) is a process to capture CO_2 and store it in geologic reservoirs. In this process, CO_2 is captured, then injected 1 to 4 kilometers below the land surface into porous rock formations. According to the U.S. Department of Energy (2009), depleted oil and gas reservoirs could store as much as 82 billion metric tons of CO_2 and saline ground water reservoirs could store as much as 3400 billion metric tons of CO_2. Because they are widespread, unused, and have high storage capacity, deep saline aquifers are generally regarded as the most attractive targets for storage of CO_2, but storage potentials and efficiencies of the GCS process must first be assessed.

STOMP (Subsurface Transport Over Multiple Phases) is a numerical modeling tool developed by the Pacific Northwest National Laboratory (PNNL). It simulates subsurface flow and transport processes in variably-saturated porous media and has been employed to model CO_2 injection into target reservoir formations (Hou et al., 2013). STOMP (White and Oostrom, 2006) requires petrophysical input properties of the formation such as porosity, intrinsic permeability, and capillary pressure–saturation parameters in order to simulate CO_2 flow and sequestration (Khudaida and Das, 2014). Accurate values of these physical properties are necessary for meaningful simulations. Gragg et al. (2012) performed a sensitivity analysis of petrophysical parameters used for numerical modeling of CO_2 with STOMP. They found that simulations were most influenced by intrinsic permeability, the van Genuchten *m* parameter, and the Brooks and Corey residual gas saturation.

Determination of capillary pressure–saturation functions that accurately characterize fluid flow in a formation can be difficult. The most common methods for determination of the capillary pressure–saturation function result in an average capillary pressure-average saturation function, $<\theta>(\psi)$, instead of the point capillary pressure-saturation function, $\theta(\psi)$. Use of the average function rather than the point

function in flow and transport models can produce erroneous predictions of important hydraulic properties such as the relative permeability function (Peters and Durner, 2006). Cropper et al. (2011) demonstrated that use of the average function rather than the point function significantly affected capillary pressure–saturation functions measured by steady state centrifugation.

Petrophysical properties of Berea Sandstone including porosity, intrinsic permeability, and both average and point capillary pressure-saturation functions determined by steady-state centrifugation were measured for Chapter 2 (Cropper et al, 2011). For this paper, these measured petrophysical parameters will be used to simulate injection of CO_2 into a confined Berea Sandstone aquifer using STOMP. The main objective of the paper is to compare STOMP simulations using point capillary pressure-saturation function, $\theta(\psi)$, parameters to simulations using average capillary pressure-saturation function, $\langle\theta\rangle(\psi)$, parameters when all other parameters in the model remain constant. This comparison will test the hypothesis that numerical simulations using point functions are different from simulations using average functions.

Materials and Methods

Petrophysical Properties

Berea sandstone was selected as the material for simulation in this investigation. It is a consolidated siliciclastic rock from Ohio widely employed as standard material in petroleum engineering. Three cylindrical sandstone cores (3.80 cm diameter, 4.78 cm length) were supplied by Coretest Systems, Morgan Hill, CA. Intrinsic permeability, k, and porosity, ϕ, of the sandstone core samples are shown in Table 7. The samples were saturated and centrifuged with a URC-628 Ultra-Rock Core centrifuge (Coretest Systems, Morgan Hill, CA) as described in detail by van den Berg et al. (2009). The steady state centrifuge outflow data was analyzed to produce both point capillary pressure-saturation function, $\theta(\psi)$, parameters and average capillary pressure-saturation function, $\langle\theta\rangle(\psi)$, parameters as described in detail by Cropper et al. (2011). The resulting average and point capillary pressure–saturation van Genuchten (1980) parameters are shown in Table 8.

STOMP Simulation Scenario

The following assumptions were made for all simulations that follow: The modeled formation was a 100 m thick layer of Berea sandstone. It was an isotropic and homogeneous aquifer of 100 km radial extent. For each simulation, supercritical CO_2 was injected at a constant rate into the center of the formation which behaved as an infinite-acting domain. The duration of injection was 10,000 days (~27 years). The initial pressure was 12 MPa which corresponded to a depth of ~1200 m. The initial aquifer salinity was 15 weight percent sodium chloride. The initial aquifer pressure was 12 MPa. The initial aquifer temperature was 45^o Celsius. A constant flux boundary was set at the injection side, a constant head boundary was set at the opposite side, and no-flow boundaries were set at the formation top and bottom. One hundred grid cells were defined in the model, with spacing increasing exponentially with distance from the injection well. Gravity and inertial effects were neglected in this model. Flow was assumed to be exclusively one-dimensional. It was also

assumed that the sandstone would not fail at the buildup pressures achieved during the simulation. This base scenario was created following Cheng et al. (2013), who followed Pruess et al. (2002).

Data Analysis

For each simulation, an input file was prepared that contained values of intrinsic permeability, k, porosity, ϕ, the van Genuchten (1980) capillary pressure–saturation parameters (α, m, and S_r) and a CO_2 injection rate. After the STOMP program completed the simulation, it produced an output file containing the gas pressure at each of 100 grid cells in the model. These gas pressures were then averaged to determine the mean gas pressure associated with that flow rate. Two sets of aquifer parameters were compared: 1) using the intrinsic permeability, k, and porosity, ϕ, in Table 7 and the measured average van Genuchten (1980) capillary pressure–saturation parameters (α, m, and S_r) in Table 8 – henceforth referred to as the average simulation and 2) using the intrinsic permeability, k, and porosity, ϕ, in Table 7 and the measured point van Genuchten (1980) capillary pressure–saturation parameters (α, m, and S_r) in Table 8 – henceforth referred to as the point simulation. Eight injection flow rates (3.13, 6.25, 12.5, 18.75, 21.88, 25, 50, and 100 kg s^{-1}) were used for both of the simulation scenarios producing a total of 16 simulations. Although the flow rate was changed for each of the 16 simulations, it was held constant during each individual simulation.

Results and Discussion

Point Simulations Compared to Average Simulations

The data set of eight flow rates and their associated mean gas pressures produced by the average simulations were compared to the data set of eight flow rates and their associated mean gas pressures produced by the point simulations. Table 9 contains mean gas pressures produced by simulations of each injection flow rate for the simulation sets, and Figure 9 compares the average and point simulations

graphically. In both cases the mean gas pressure is a linear function of the injection flow rate ($R^2 > 0.996$ for both simulation sets) across the range of injection flow rates simulated, so injection flow rates at any mean gas pressure can be estimated from the ratio of the slopes of the trend lines. The point simulation parameters predict higher injection rates for all gas pressures higher than 1.22×10^7 Pa compared to the average parameters. Based on the ratio of line slopes, point injection flow rates are 136% of the average injection rates across the range of flow rates simulated. The average parameters underestimate the rate at which CO_2 could be injected at all gas pressures simulated. For example, at a mean gas pressure of 1.5×10^7 Pa (2176 PSI), the flow rate predicted by the average simulation parameters is 35.938 kg s^{-1} compared to 48.268 kg s^{-1} predicted by the point function parameters. Use of the average parameters instead of point parameters in this example would underestimate the mass of CO_2 injected by 1065 metric tons per day. A practical implication of these simulations is that simulations using point parameters show larger increases in injection flow rates for a given increase in gas pressure when compared to simulations using average parameters.

The Impact of Flow Rate on Injection Cost Estimates

Heath et al. (2012) estimated the annual cost of operation of a 7,000 feet deep injection well to be $876,483 in 2010 dollars. After adjustment for inflation (assuming 1.09% cumulative inflation) the 2014 daily operating cost is $2694. Because the cost of operation of an injection well is a function of time and not the CO_2 injection flow rate, injection at a higher flow rate decreases the cost per ton of CO_2 injected without increasing operating costs. As a result, accurate estimates of attainable injection flow rates will produce more exact assessments of the true cost of geologic carbon sequestration. For example, at a mean gas pressure of 1.5×10^7 Pa, the average simulation parameters predict a flow rate of 35.939 kg s^{-1}, which would inject 2105 metric tons of CO_2 per day of operation. Using the daily operating cost to calculate injection efficiency yields an efficiency of $0.87 per metric ton of CO_2 injected. The

same type of analysis for the same mean gas pressure, using the point simulation parameters rather than the average simulation parameters yields a flow rate of 48.268 kg $s^{-1.}$ Operating at this flow rate would inject 4170 metric tons of CO_2 per day of operation, at a much more efficient cost of $0.65 per ton injected. Table 10 compares injection flow rates, CO_2 injected per day, and injection efficiency in terms of dollars per ton of CO_2 injected.

Conclusions

Deep saline aquifers are attractive targets for long-term storage of CO_2, but the preliminary simulations completed in this paper suggest that reliable estimates of attainable injection flow rates and storage cost efficiencies will require accurate estimates of formation petrophysical properties. Simulations using porosity, intrinsic permeability, and point van Genuchten parameters determined in Berea sandstone predicted mean flow rates 1.36 times higher than simulations using average capillary pressure-saturation function parameters in the same material while holding all other parameters constant. Because of the lack of available research on the appropriate scale for the capillary-pressure saturation function in large-scale numerical simulations, we cannot say that the point parameter set produces a more accurate simulation compared to the average parameter set. However, the simulations do show that even relatively small variations in capillary pressure-saturation parameters due to scale can have significant effects on predicted flow rates and injection efficiencies. If numerical simulations such as these are used to determine the viability of long-term CO_2 storage projects it will be important to accurately determine petrophysical input properties including capillary pressure-saturation parameters. Research on the appropriate scale of these parameters for inclusion in large-scale numerical simulations also deserves further attention.

References

Cheng, C-L., M. J. Gragg, E. Perfect, M. White, P. J. Lemiszki, and L. D. McKay. 2013. Sensitivity of injection costs to input petrophysical parameters in numerical geologic carbon sequestration models. International Journal of Greenhouse Gas Control 18: 277-284.

Cropper, S. C., E. Perfect, E. H. van den Berg, and M. A. Mayes. 2011. Comparison of average and point capillary pressure–saturation functions determined by steady-state centrifugation. Soil Science Society of America Journal 75(1):17-25.

Gragg, M. J., 2012. CO_2 Injection into a deep saline aquifer: porosity measurements, numerical modeling, and costs associated with uncertainty of petrophysical parameters. Master's Thesis, University of Tennessee.

Heath, J. E., P. H. Kobos, et al. 2012. Geologic Heterogeneity and Economic Uncertainty of Subsurface Carbon Dioxide Storage. SPE Econ & Mgmt. 4(1): 32-41. SPE158241PA.

Hou, Z., Engel, D. W., Lin, G., Fang, Y., & Fang, Z. 2013. An uncertainty quantification framework for studying the effect of spatial heterogeneity in reservoir permeability on CO2 sequestration. Mathematical Geosciences, 45(7), 799-817.

Khudaida, K and D.B Das, 2014. A numerical study of capillary pressure-saturation relationship for supercritical carbon dioxide (CO_2) injection in deep saline aquifer. Chemical Engineering Research and Design, in press, doi: 10.1016/j.cherd.2014.04.020.

Peters, A., and W. Durner. 2006. Improved estimation of soil water retention characteristics from hydrostatic column experiments. Water Resour. Res. 42:W11401, doi: 10.1029/2006WR004952.

Pruess, K., J. Garcia, et al. (2002). Intercomparison of numerical simulation codes for geologic disposal of CO_2. NETL, LBNL---51813: 104 pages.

U.S. Department of Energy, National Energy Technology Laboratory, 2009. Carbon sequestration atlas of the United States and Canada, 2d ed. http://www.netl.doe.gov/technologies/carbon_seq/refshelf/atlas/.

van den Berg, E.H., E. Perfect, C. Tu, P.S.K. Knappet, T.P. Leao, and R.W. Donat. 2009. Unsaturated hydraulic conductivity measurements with centrifuges: A review. Vadose Zone J. 8:531–547.

van Genuchten, M.Th . 1980. A closed-form equation for predicting the hydraulic conductivity of unsaturated soils. Soil Sci. Soc. Am. J. 44:892–898.

White, M. And M. Oostrom, 2006. "STOMP Subsurface transport over multiple phases, version 4.0, User guide." Richland, Washington, Pacific Northwest National Laboratory.

Appendix III-A Tables

Table 7. Physical properties of porosity (ϕ), and intrinsic permeability (k) for the Berea sandstone cores.

Sample-replicate no.	Φ (m3 m^{-3})	k (m^2)
Berea-1	0.183ǂ	1.73×10^{-9}ǂ
Berea-2	0.182ǂ	1.19×10^{-9}ǂ
Berea-3	0.188ǂ	2.23×10^{-10}ǂ
Average of 3 Samples	0.184	1.05×10^{-9}

ǂ Data supplied by Coretest Systems, Morgan Hill, CA.

Table 8. Summary of van Genuchten (1980) estimates of the residual saturation, S_r, and α, n, and m parameters for the average and point methods fit to centrifuge retention data for Berea sandstone core samples (Cropper et. al, 2011).

Sample-replicate no.	Method	S_r	α (k Pa^{-1})	n	m (=1-1/n)
Berea-1	Average	0.178	0.087	1.893	0.472
Berea-2	Average	0.160	0.131	1.671	0.402
Berea-3	Average	0.143	0.119	1.658	0.397
Average of 3 Samples	Average	0.160	0.112	1.741	0.423
Berea-1	Point	0.184	0.076	2.442	0.590
Berea-2	Point	0.169	0.120	1.920	0.479
Berea-3	Point	0.155	0.108	1.913	0.477
Average of 3 Samples	Point	0.169	0.101	2.092	0.516

Table 9. Mean gas pressures corresponding with each simulated injection flow rate for the point and average simulation sets.

Flow Rate ($kg\ s^{-1}$)	Mean Gas Pressure Point Simulations (Pa)	Mean Gas Pressure Average Simulations (Pa)
3.13	1.23×10^7	1.38×10^7
6.25	1.25×10^7	1.53×10^7
12.50	1.30×10^7	1.84×10^7
18.75	1.33×10^7	2.13×10^7
21.88	1.36×10^7	2.28×10^7
25.00	1.37×10^7	2.42×10^7
50.00	1.53×10^7	3.57×10^7
100.00	1.79×10^7	5.81×10^7

Table 10. Injection flow rates, mass of CO_2 injected per day, and dollars per ton of CO_2 injected compared for two simulation parameter sets injected at mean gas pressures of 1.5×10^7 Pa.

Simulation	Flow Rate ($kg\ s^{-1}$)	CO_2 Injected ($t\ d^{-1}$)	Injection Efficiency ($\$\ t^{-1}$)
Average	35.938	2105	0.87
Point	48.268	4170	0.65

Appendix III-B Figures

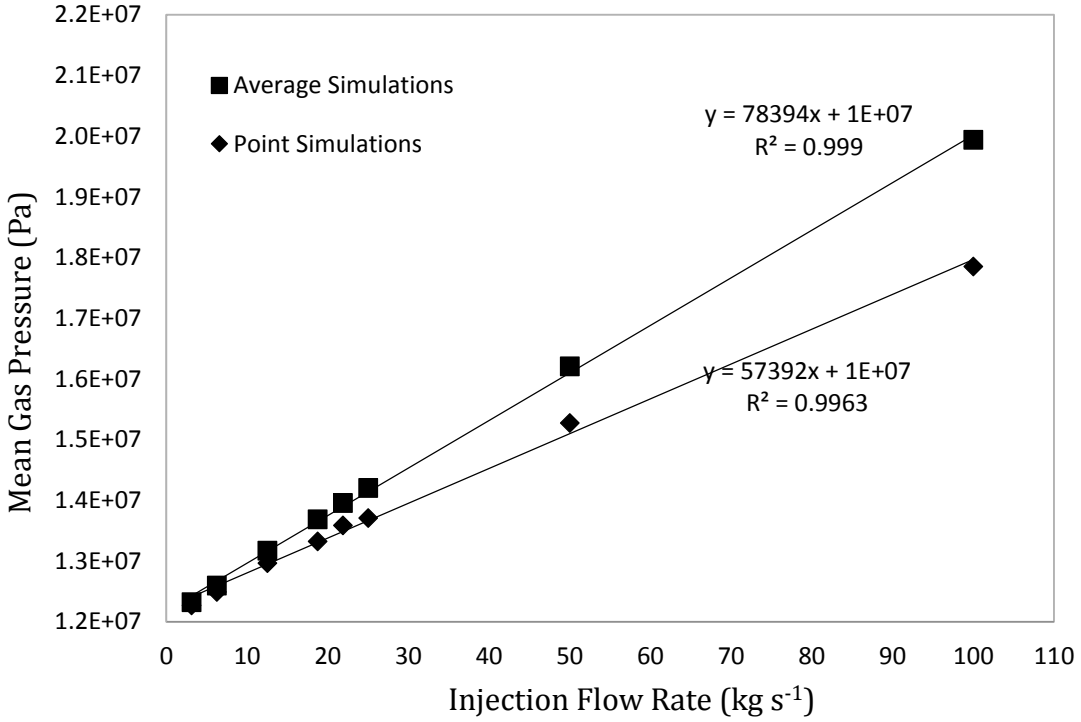


Figure 9. Comparison of mean gas pressures resulting from simulations using average simulation parameters and mean gas pressure resulting from simulations using point simulation parameters at eight injection flow rates.

Chapter IV

Comparison of Upscaled and Measured Capillary Pressure – Saturation Parameters for Flint Sand

This chapter has not previously been published, nor will it be before the final version of this dissertation is submitted.

Samuel Clark Cropper contributed to this chapter by performing the laboratory experiments and data analysis and writing the paper. Others contributed by revising the manuscript.

Abstract

The capillary pressure-saturation function is a key hydraulic function used to characterize water retention in the vadose zone. It is scale dependent. Standard methods used to determine capillary pressure–saturation behavior produces average saturation versus average pressure potential functions for the sample, <S>(<ψ>), rather than point, S(ψ), functions. Neutron imaging can measure the point, S(ψ) function directly. Analytical expressions exist that can relate point, S(ψ), functions to average, <S>(<ψ>), functions. These expressions can be used to upscale point, S(ψ), parameters to produce average, <S>(<ψ>), parameters at any scale of interest assuming the porous medium is homogeneous, and to produce point, S(ψ), parameters inversely from average, <S>(<ψ>), parameters. The purpose of this paper is to compare upscaled predictions of average <S>(ψ) functions to measured average <S>(ψ) functions in Flint sand. Average <S>(ψ) functions for nine different column lengths between 4.3 cm and 55.0 cm were predicted from point, S(ψ), functions determined by neutron imaging of Flint sand. These predictions were compared to average <S>(ψ) functions determined by the hanging column method. The results show that upscaled functions were generally good predictors of observed average, <S>(<ψ>), functions for the column lengths measured, but only if the pressure reference elevation for the upscale analysis is adjusted to the top of the column in the upscaler algorithm. The van Genuchten α and *n* parameters of the upscaled predictions correlate well with the observed α and *n* parameters after this adjustment. Upscaled predictions of residual saturation did not correspond with observed values even after the pressure reference was adjusted. Inverse predictions of point, S(ψ), parameters from observed average, <S>(<ψ>), retention data produced variable results when compared to point S(ψ), parameters measured by neutron imaging. Few parameters fell within the 95% confidence limits of the neutron estimates, and deviations were large for some column lengths.

Introduction

The hydraulic properties of natural porous media commonly display scale dependency. As a result, measurements of hydraulic properties obtained at one scale must be upscaled or downscaled to predict behaviors at a different scale. Vereecken et al. (2007) review various scaling approaches. Common examples include forward predictions of field-scale contaminant transport within a soil profile based on measurements of hydraulic properties measured at a local scale, and inverse estimation of effective hydraulic parameters from the application of small-scale constitutive equations to field-scale data sets. These examples relate local scales to field scales, but scaling can also be from one local scale to a different local scale. In this document both upscaling and downscaling are evaluated at local scales.

The water retention function, $S(\psi)$, is a key hydraulic function used to characterize water retention in the vadose zone and to predict relative permeability. Parameters describing the $S(\psi)$ function are needed as model inputs for simulating a variety of critical issues related to the environment (e.g., permafrost thawing due to climate change) and energy (e.g., geologic carbon sequestration in confined brine aquifers). The $S(\psi)$ function is most often determined at a local scale experimentally by observing changes in saturation of a sample of finite length (typically < 3 cm) as it is subjected to a series of step changes in pressure in a pressure cell, hanging water column, or centrifuge. Hydraulic parameters obtained by such methods are scale dependent (Liu and Dane, 1995a). If the distribution of liquids within the sample is unknown, the water retention function at any physical point in the sample, $S(\psi)$, is also unknown. As a result, these experiments produce an average saturation versus average pressure potential function for the sample, $\langle S \rangle(\psi)$, rather than the point, $S(\psi)$, function. Parameters describing $\langle S \rangle(\psi)$ depend upon the column/layer height over which the averaging has been measured. Average $\langle S \rangle(\psi)$ functions can differ significantly from point, $S(\psi)$ functions (Cropper, et al. 2011).

The water retention function, $S(\psi)$ can be measured by other methods, including methods that directly measure the point function at different locations

within the sample. Sakaki and Illangasekare (2007) simultaneously measured point and average capillary pressure-saturation functions using a modified Tempe cell with a time domain reflectometry (TDR) probe inserted horizontally midway between the top and bottom of the cell. Vasin (2008) showed that it is possible to measure water retention functions on heterogeneous materials at different scales using neutron imaging. Cheng et al. (2012) employed neutron radiography to measure average water retention functions on homogeneous soil columns packed with Flint sand. Kang et al. (2014) employed neutron radiography to determine 120 point S(ψ) functions at different spatial locations within a column of Flint sand.

Liu and Dane (1995a) derived analytical expressions, based on height-averaging, that relate point, S(ψ), functions to the average function, <S>(<ψ>):

$$\psi = \langle\psi\rangle + z_n \frac{\rho_n}{\rho_w} - z_w + \left(1 - \frac{\rho_n}{\rho_w}\right) z \qquad [7a]$$

$$\langle S\rangle = \frac{1}{z_c}\int_0^{z_c} S(\psi) dz \qquad [7b]$$

where ‹ψ› (m) is the average capillary pressure, <S> (dimensionless) is the height averaged relative saturation, ψ (m) is the point capillary pressure, S (dimensionless) is the point relative saturation, z_n (cm) and z_w (m) are the heights where the pressures of the non-wetting (i.e. air) and wetting (i.e. water) fluids are measured respectively, z (m) is the height at a point, z_c (m) is the column height, and ρ_n (g cm^{-3}) and ρ_w (g cm^{-3}) are the densities of the non-wetting and wetting fluids respectively. Equation [7] allows inverse determination of point functions from average functions obtained using experimental methods such as a pressure cell, or forward predictions of average functions for columns of any height from point functions determined using experimental methods such as neutron imaging.

Liu and Dane (1995b) used Equation [7] to compute point functions from average pressure cell retention data. Jalbert et al. (1999) developed a computer program (TrueCell) that inversely estimates point hydraulic parameters from <S>(ψ)

data based on Equation [7]. Cheng et al. (2013) also used Equation [7] as the basis of a computer program, the BC-vG Upscaler, that upscales point BC S(ψ) parameters to any scale of interest assuming the porous medium is homogeneous. The BC-vG Upscaler implements the Liu and Dane (1995a) approach in a forward manner and then parameterizes the resulting scale dependent <S>(ψ) relationships using the van Genuchten (1980) equation (vGE). Forward predictions of the BC-vG Upscaler have not been experimentally verified.

The objectives of this paper are to test two hypotheses related to Equation [7]: (i) measured point capillary pressure-saturation retention data can be upscaled with the BCvG Upscaler to predict average functions; and (ii) measured average capillary pressure-saturation retention data can be downscaled with TrueCell to predict point functions. Accomplishing these objectives will require two kinds of experiments and several processing/parameterization steps as follows: (i) measure water retention in Flint sand columns of various lengths using hanging water columns and parameterize the VGE average, <S>(ψ), functions; (ii) use BC point, S(ψ), parameters determined by neutron imaging and the BC-vG Upscaler to predict VGE average <S>(ψ) functions for flint sand columns for the observed lengths; (iii) compare forward predicted (BC-vG Upscaled) VGE average function parameters to observed VGE function parameters at several local scales; (iv) use TrueCell to inversely determine point BCE functions from the observed retention data; and (v) compare inversely predicted TrueCell point BCE function parameters to point BCE parameters determined by neutron imaging. A conceptual diagram relating the laboratory experiments, data parameterizations, and comparisons of predictions and observations is shown in Figure 10.

Materials and Methods

Hanging Water Column Experiments

Flint sand (Flint #13, U.S. Silica Company, Berkeley Springs, WV) was selected as the material for this study. It is a relatively coarse homogeneous porous medium that should have minimum pressure equilibrium times over the range of column lengths studied. Sand grain diameters for this material range from 0.11 to 0.60 mm with a median grain diameter of 0.56 mm. The material is mainly composed of quartz (99.8%), has a particle density of 2.65 g cm^{-3}, and saturated hydraulic conductivity of $1.66 \pm 0.32 \times 10^{-4}$ m s^{-1} (U.S. Silica Product Data Sheet, 2009).

The hanging water column setup (Figure 11) consisted of clear ¾ inch PVC pipe (inner diameter = 1.83 cm) connected with Tygon tubing via an outlet at its base to a burette filled with water. A pressure transducer (PX409USB, Omega®, Manchester, UK) was attached to the burette and set to record cumulative water outflow at regular time intervals ranging from 1 to 30 seconds. The bottom of the clear PVC pipe was covered with four layers of moist Whatman #4 filter paper to provide a phase barrier. The column was filled with water and any air bubbles in the hanging water column setup were removed. Flint sand was incrementally added to the water in the column in ~4 cm layers and the column was tapped to minimize air entrapment until the sand column reached the desired height. The completed sand columns were fully saturated with water by raising the water level in the burette to a height equal to the top of the sand pack, or slightly higher, and allowed to equilibrate overnight prior to drainage.

Prior to each drainage experiment, the fully saturated sand columns were clamped to a stationary stand. The sand columns were drained stepwise by lowering the hanging water setup on an adjustable stand. Steps were typically ~3 cm, but were increased up to ~15 cm if low water outflow indicated that residual saturation had been achieved. After each step, and at intervals between steps, the water level in the hanging water column burette, the volume of water in the burette, and the transducer

outflow reading was recorded and later used to construct the main drainage curve. A real-time graphic display of outflow reported by the pressure transducer was used to judge when quasi-equilibrium conditions had been reached for each increment. Drainage continued in this matter for each column until air passed the phase barrier. After drainage was complete, the column sand was oven dried for 24 h at 105^0 C and weighed for bulk density and porosity calculations.

The hanging water column retention data were parameterized using the "constrained" form of the van Genuchten (1980) equation:

$$S = (1 - S)[1 + (\alpha\psi)^n]^{-\left(1-\frac{1}{n}\right)} + S_r \qquad [8]$$

where S_r is residual saturation (dimensionless), and α (Pa^{-1}) and n are empirical parameters. The S_r, n and m parameters in Equation [8] were fitted to the drying curve data using nonlinear regression (Marquardt method) in SAS 9.4 (SAS). The goodness of fit was assessed based on the root mean square error (RMSE).

Neutron Point BC Parameterization

Neutron imaging is a nondestructive method for measuring water content based on measuring the transmitted intensity of neutrons through a porous medium (Perfect et al., 2014). Neutrons are attenuated differently by hydrogen and mineral solids. Water thickness can be determined by observing the attenuation of neutrons transmitted through a sample, and the water content at any physical point can be derived from the measured water thickness at that point. The capillary pressure-saturation behavior at any point in the sample can then be determined by observing changes in water thickness during quasi-equilibrium drainage increments, as related to the known distribution of capillary pressures within the column.

Kang et al. (2014) conducted neutron imaging experiments to characterize the point S(ψ) drainage behavior of a 5.6 cm tall column of Flint sand using a hanging water setup and quasi-equilibrium drainage technique very similar to the

experimental methods described in the previous section. They processed the neutron imaging water content data into a grid of 120 point locations during 9 imposed quasi-equilibrium suction increments to produce 1080 paired observations of point water content at capillary pressures between 2.66 cm and 47.27 cm. For the present research, this data set was parameterized to the Brooks and Corey (1964) equation by fitting all 1080 data pairs to produce a composite point S(ψ) function for Flint sand. The BC equation was fitted in the following form:

$$S = (1 - S_r)\left(\frac{\psi_a}{\psi}\right)^{\lambda} + S_r \quad \{\psi > \psi_a\} \qquad [9a]$$

$$S = 1 \qquad \{\psi \leq \psi_a\} \qquad [9b]$$

where ψ_a is the air entry value (kg m^2 s^{-2}), S_r is the residual saturation (dimensionless), and λ is the pore-size distribution index. Equation [9] was fitted to the neutron imaging data using segmented nonlinear regression (Marquardt method) in SAS 9.4 (SAS). The goodness of fit was assessed based on the root mean square error (RMSE).

BC-vG Upscaler Predicted vGE Average Functions

The BC-vG Upscaler program (Cheng et al., 2012) was used to predict average vGE parameters for each column length using the point BC parameters produced by parameterization of the neutron data of Kang et al. (2014) as initial parameter estimates and the *m*=1-1/*n* fitting option. The BC-vG Upscaler generates 120 height-averaged capillary pressure head values (cm) ranging between $\psi_a \times 10^{-2}$ and $\psi_a \times 10^{4}$ spaced logarithmically to intensely cover the air-entry and rapid drainage portions of the retention curve. The Upscaler software assumes that elevations of known pressure for both wetting and nonwetting fluid phases is at the midpoint of column length, and then predicts an average saturation for each generated suction value using Equation [7]. This generated retention set of 120 data points is then parameterized using Equation [8] (Cheng et al. 2012).

TrueCell Point BC Parameterization

TrueCell (Jalbert et. al, 1999) was used to inversely extract BC point parameters from the average water retention data observed during drainage of each column. TrueCell requires column configuration details including column length, z_c, the position where nonwetting fluid pressure was measured relative to the bottom of the column, z_n, the position where wetting fluid pressure was measured relative to the bottom of the column, z_w, and the densities of the non-wetting and wetting fluids. For all the hanging water columns the known pressure elevations were the top of the column. As a result, $z_w = z_n = z_c$. Fluid densities for all columns were assumed to be 0.001 g cm^{-3} and 1.000 g cm^{-3} for ρ_n (air) and ρ_w (water) respectively. Point BC parameters produced by parameterization of the neutron data of Kang et al. (2014) were used as initial estimates for fitting parameters.

Results and Discussion

Hanging Water Column Experiments

A total of eleven Flint sand columns were prepared and drained using the hanging water column method. Data pairs of capillary pressure and saturation were collected at each quasi-equilibrium step. Data from one hanging water column performed by Kang (personal communication) using the same Flint sand and the same experimental technique are also included. Air passed the phase barrier prior to reaching residual saturation during drainage of three columns leaving nine water retention data sets with sand column lengths ranging from 4.3 cm to 55.0 cm. Table 11 contains completed column lengths, bulk density (= mass of oven dry sand/total volume of the packed sand column), porosity (= 1 - bulk density/particle density), and recording time interval of each sand column. Porosity ranged between 0.326 and 0.390 with a mean of 0.350. The nine complete data sets contain at minimum 15 and as many as 25 equilibrium steps. Drainage durations ranged from 5 hours (4.3 cm column) to ~12.5 days (55.0 cm column). Table 12 shows the number of capillary pressure increments, the range of capillary pressures, and total drainage time for

each column. Equilibrium steps above the air-entry pressure were easy to distinguish using the graphic display of water outflow. Figure 12 shows the pattern of outflow equilibrium steps for selected columns.

Forward Predictions of Average vGE Parameters from Point Parameters

Equation [9] was fitted to complete data set of 120 retention pairs determined by neutron imaging by Kang et al (2014) using segmented nonlinear regression (Marquardt method) in SAS 9.4 (SAS). The resulting parameters and goodness of fit assessed based on the root mean square error (RMSE) are shown in Table 13. Approximate standard errors for each parameter are shown in parentheses. These parameters were interpreted as the point BC characteristics of the Flint sand, and are used in the BC-vG Upscaler as the basis for forward predictions. Predicted average parameters produced by the BC-vG Upscaler for various column lengths are shown in Table 14.

The observed retention data set for each column was parameterized using Equation [8] to produce average vGE parameters shown in Table 15. Saturation was calculated as a percentage of the maximum water content (S= equilibrium water content/maximum water content) and was not fit. Residual saturation was set to the minimum observed saturation for each drainage experiment and was not fitted. Predicted parameters from Table 14 were used as initial estimates for parameterization of hanging column retention data sets in all cases except for the 37.0 cm column. Parameterization of the data for that column with the predicted parameters as initial estimates produced large errors. Figure 13 compares upscaled average vGE function predictions (red) to observed retention data points (blue) and van Genuchten fits to the observed retention points (green). Agreements are relatively good for the shortest column length, 4.3 cm, but degrade with increased column length and are very poor for the longest columns. Figure 14 compares observed relative saturation values to relative saturation values predicted by the BC-vG Upscaler. Most data points fall far from the 1:1 line indicating little correspondence

between observations and predictions. Figure 15 compares predicted parameters to observed parameters. The BC-vG upscaler over-predicted the observed α parameters for all column lengths. The trend line through the plotted α parameters in Figure 15 has slope = -0.353 indicating no correlation between predicted and observed values. The upscaler under predicted the observed *n* parameters for all column lengths except the shortest one (4.3cm). Predicted saturations ranged from 0.88 to 1.00. Residual saturations predicted by the upscaler vary little with column length, 0.058 to .065. In contrast, the residual saturations fit to the retention data show much more variation with column length, 0 to 0.14. Clearly, the BC-vG Upscaler predicted neither the saturation functions nor the individual function parameters.

An assumption made by the BC-vG Upscaler is that both wetting and nonwetting fluid pressures are known at mid-column, but a mid-column pressure reference was not used for analysis of the hanging column retention data. A mid-column reference complicates analysis of retention data produced by the hanging column method. When the nonwetting fluid phase has lower density than the wetting phase, as is the case for the water and air used in this study, the non-wetting phase fluid enters at the top of the column as wetting phase fluids drains from the bottom. Saturation remains at a value of 1 in the hanging column until air enters the column at the top, then decreases until residual saturation is attained. If a mid-column reference is assumed for this drainage, saturation remains 1 at mid-column for some time after the nonwetting phase has entered the column top, misrepresenting the saturation as 1 when the average saturation for the column is actually less than 1. If all drainage data produced during the hanging water experiment is considered, capillary pressure at mid-column is negative during early drainage and only becomes positive during continued drainage. Equation [8] cannot accurately parameterize drainage data sets containing both positive and negative capillary pressures. On the other hand, if early drainage data points with negative pressures are discarded, the data set is incomplete, and Equation [8] would not be expected to accurately parameterize an incomplete drainage set. For these reasons, a top column pressure

reference was used to parameterize the hanging water column data sets in this study. However, the mismatch in pressure reference (i.e. mid-column elevation reference used by the upscaler vs top-column reference used for the hanging water columns) could be the cause of the poor agreement observed between upscaled predictions and observed drainage behavior.

To investigate the effect of pressure reference on predictions made by the BC-vG Upscaler, the upscaler parameterization procedure was replicated using top, middle, and bottom pressure references. As is done by the BC-vG Upscaler, 120 height-averaged capillary pressure head values ranging between $\psi_a \times 10^{-2}$ and $\psi_a \times 10^4$ cm were generated and average saturation was predicted at each value using Equation [7] and using the point BC parameters in Table 13. Figure 16 shows the effect for each of the hanging column lengths and the range of pressures observed in this study. For the shortest column lengths, saturation and residual saturation values agree on all three curves, but there are small differences in predicted behavior during column drainage. While the 4.3 cm and 14.4 cm columns both produce full drainage data sets for any elevation reference within the column, column lengths longer than these fail to produce complete data sets for a bottom reference (red). Columns shorter than 37.0 cm produce full drainage data sets for middle column references (green), but longer columns do not. The results of parameterization of incomplete drainage sets generated by this algorithm can be observed on the longest three column lengths in Figure 16. The middle column reference predictions (green) for these three columns lack any retention data pairs with saturations near 1. It is doubtful that parameterizing a data set lacking information about column conditions at saturation could accurately characterize the sample retention behavior.

Based on this analysis, the BC-vG Upscaler algorithm was modified to generate top-referenced data sets for each hanging column length using the point parameters in Table 13. While no single pressure elevation can accurately characterize the range of pressures through a tall column, a top reference produces a full retention data set for parameterization, and might be a better comparison to the hanging water column

retention data which was based on a top pressure reference. The resulting retention data sets were parameterized using Equation [8] and nonlinear regression (Marquardt method) in SAS 9.4 (SAS) which is consistent with the mid column reference procedure. The goodness of fit was assessed based on the root mean square error (RMSE). The parameters resulting from this analysis are shown in Table 16. Figure 17 shows the upscaled predictions based on a top pressure reference (orange) overlain on the mid pressure reference and observed drainage data previously shown in Figure 17. The top pressure reference predictions show considerably better agreement with the observed data when compared to the mid pressure reference for all column lengths. Figure 18 compares observed relative saturation values to relative saturation values predicted by the BC-vG Upscaler after adjustment to a top pressure reference. The trend line corresponds well with the 1:1 line (slope =1.03; R^2=0.98) confirming the generally good agreement observed in Figure 13. For most column lengths, the predictions agree very well with the observed data. However, the top reference predictions for several column lengths disagree on the dry end of the curve. This is most evident on the 14.4 cm and 24.9 cm columns. Figure 19 compares the individual van Genuchten (1980) predicted parameters to observed parameters. The α parameters show close correspondence (slope = 0.96). The predicted *n* parameters show less correspondence (slope = 0.78) and in most cases slightly over predict the observed n parameters. All values of predicted and observed saturations are clustered at 1, but there is disagreement between the predictions of residual saturations from the observed values. The upscaled predictions vary over a small range (0.06 to 0.07), but the residual saturations fit to the observed data vary over a much larger range (0 to 0.14)

Inverse Predictions of Point Parameters from Average Data

The average capillary pressure-saturation data sets collected during drainage of each column were processed in TrueCell (Jalbert et. al, 1999) to extract BC point parameter estimates for each column. The resulting parameters and goodness of fit

assessed based on the root mean square error (RMSE) are shown in Table 17. Neutron point BC estimates from Table 13 are included for comparison. Figure 20 compares the TrueCell point BC parameter estimates to the point BC parameters fit to the neutron imaging data of Kang et al, (2014). Neutron parameters are shown as dashes with 95% confidence limits as gray bars. Only the 19.7 cm column had predicted residual saturation within the 95% confidence limits of the neutron imaging value. Estimates for all other columns over predicted the residual saturation. The maximum deviation was +0.096 for the 24.9 cm column. The 95% confidence limit for the air-entry, (ψ_a), parameters was a very small range (±0.12). No columns had estimates of ψ_a that fell within the 95% confidence limits. The maximum deviation for ψ_a was +3.051 kPa for the 14.4 cm column. Air entry estimates for all other columns under predicted the neutron air entry value. The 95% confidence range was also small (±0.51) for the pore size distribution index, λ. The parameter estimate of λ for one column, 48.5 cm, fell within this range. The maximum deviation for λ was +22.983 for the 37.0 cm column, but this was much higher than all other deviations of λ.

Discussion and Conclusions

The objectives of this paper were to test two hypotheses related to Equation [7]. The first hypothesis was that measured point capillary pressure-saturation retention data can be upscaled with the BCvG Upscaler to predict average functions. To test this hypothesis, point functions determined by neutron imaging were upscaled to produce estimated average functions and these were compared to average functions determined by the hanging column method. Initially, the BC-vG Upscaler algorithm generated partial retention data sets for columns longer than 37 cm and parameterization of these partial data sets produced unacceptable fits to the observed data as shown in Figures 13 and 15. Predicted parameters did not correlate to observed parameters. However, after an adjustment of the pressure reference, the BCvG algorithm generated full retention data sets and significantly improved fits over

the mid pressure reference predictions (Figures 17 and 18). This agreement supports the first hypothesis above, as well as the BC-vG algorithm, and the Liu and Dane (1995a,b) analytical expressions that the algorithm is based on.

Interestingly, the upscaled function predictions agree closely with the observed behavior even though only two of the three fitted parameters correlate well with parameters fit to the observed data. The residual saturation, S_r, parameter did not correlate well even after the algorithm was adjusted (Figure 19). This illustrates that multivariate curve fitting algorithms vary parameter sets to minimize the error of a function compared to data points, therefore it is possible that a parameter set achieves a good fit even if parameters individually may not correlate. It is worth noting how the pressure reference complication encountered during this analysis illustrates the challenges of experimental measurement of capillary-pressure drainage data.

The discrepancy between the predicted and observed residual saturations deserves further investigation. For both middle and top reference analyses, the predicted residual saturations vary over a small range close to 0.06, but observed values range between ~0.06 and ~0.16. The BCvG Upscaler algorithm consistently predicted residual saturations very close to the point residual saturation entered from the neutron measurements for column lengths between 4.3 cm and 55.0 cm. The upscaler predicted little variability in this parameter with changes in column length, but observed values varied significantly. Further testing will be required to determine if the wide range of observed residual saturations was experimental error, or if the lack of variability in the predicted residual saturations is a deficiency of the upscaler algorithm.

The second hypothesis tested was that measured average capillary pressure-saturation retention data can be downscaled with TrueCell to predict point functions. To test this hypothesis, measured average retention data sets for nine different columns lengths were processed in TrueCell to produce point BC parameters sets and these were compared to point function parameters determined by the neutron

imaging. Inverse predictions of point BC parameter sets by TrueCell produced variable results when compared to the neutron measured parameter set (Figure 20). Relatively few parameters fell within the 95% confidence limits of the neutron estimates, and some deviations were large. These results do not support the second hypothesis.

It is difficult to identify why the current study does not support the TrueCell algorithm. A previous study by Sakaki and Illangasekare (2007) found good agreement between predicted TrueCell functions and observed functions. They simultaneously measured point and average functions in the same 10 cm tall column of silica sand, processed the average drainage in TrueCell and compared the predicted point BC parameters to BC parameters determined using a time domain reflectometry probe. They found close agreement between predicted S_r and ψ_a parameters, and although there was under prediction of the λ parameter compared to the observed values of λ, the predicted saturations were generally good. It also seems contradictory that downscaling would fail to predict observed values if upscaling is able to predict observed values. Both algorithms are derived from Equation [7].

There are several possible explanations for this result. Although the current study and Sakaki and Illangasekare (2007) both used TrueCell to estimate point BC function parameters, they did not use the same method to measure the point BC functions (i.e., neutron imaging versus TDR probe, respectively). It might also be significant that average drainage behavior was measured in nine columns of variable lengths but point behavior was derived from data collected on one relatively short column (~5 cm) due to limitations on the column length that will fit into the neutron imaging setup. As a result, the upscaling involved 9 predictions as compared to results for 9 columns with their own experimental errors and variability, while the downscaling involved 9 predictions as compared to 1 experimental column with no column-to-column variability. Sakaki and Illangasekare (2007), in contrast, simultaneously measured point and average functions in the same 10 cm tall column.

Although this investigation has produced support for forward modeling with the BC-vG Upscaler, after pressure reference algorithm modifications, the variability observed in parameters produced by the TrueCell program prevents this analysis from lending similar support for the inverse modeling. Such support will require additional work.

References

Brooks, R.H., and A.T. Corey. 1964. Hydraulic properties of porous media. Hydrol. Pap. 3. Colorado State Univ., Fort Collins.

Cheng, C. L., M. Kang, E. Perfect, S. Voisin, J. Horita, H. Z. Bilheux, J. M. Warren, D. L. Jacobson, and D. S. Hussey. 2012. Average soil water retention curves measured by neutron radiography. Soil Science Society of America Journal 76(4):1184-1191.

Cheng, C-L., E. Perfect, and R. T. Mills. 2013. Forward Prediction of Height-Averaged Capillary Pressure–Saturation Parameters Using the BC-vG Upscaler. Vadose Zone Journal 12(3).

Cropper, S. C., E. Perfect, E. H. van den Berg, and M. A. Mayes. 2011. Comparison of average and point capillary pressure–saturation functions determined by steady-state centrifugation. Soil Science Society of America Journal 75(1):17-25.

Jalbert, M., J. H. Dane, and J. H. Liu. 1999. TrueCell: Physical point Brooks–Corey parameters using pressure cell data. Users guide for version 1.2. Spec. Rep. Dep. of Agron. and Soils, Auburn Univ., Auburn, AL.

Kang, M., E. Perfect, C. L. Cheng, H. Z. Bilheux, J. Lee, J. Horita, and J. M. Warren. 2014. Multiple pixel-scale soil water retention curves quantified by neutron radiography. Advances in Water Resources 65:1-8.

Liu, H.H., and J.H. Dane. 1995a. Improved computational procedure for retention relations of immiscible fluids using pressure cells. Soil Sci. Soc. Am. J. 59:1520–1524.

Liu, H.H., and J.H. Dane. 1995b. Computation of the Brooks–Corey parameters at a physical point based on pressure cell data. Spec. Rep. Dep. of Agron. and Soils, Auburn Univ., Auburn, AL.

Perfect, E., C.-L. Cheng, M. Kang, H.Z. Bilheux, J.M. Lamanna, M.J. Gragg, and D.M. Wright. 2014. Neutron imaging of hydrogen-rich fluids in geomaterials and engineered porous media: A review. Earth Sci. Rev. 129:120-135

Sakaki, T., and T.H. Illangasekare. 2007. Comparison of height-averaged and point measured capillary pressure–saturation relations for sands using a modified Tempe cell. Water Resour. Res. 43:W12502, doi:10.1029/2006WR005814.

van Genuchten, M.Th . 1980. A closed-form equation for predicting the hydraulic conductivity of unsaturated soils. Soil Sci. Soc. Am. J. 44:892–898.

Vasin, M., Lehmann, P., Kaestner, A., Hassanein, R., Nowak, W., Helmig, R., & Neuweiler, I. 2008. Drainage in heterogeneous sand columns with different geometric structures. Advances in Water Resources, 31(9):1205-1220.

Vereecken, H., R. Kasteel, Jan Vanderborght, and T. Harter. 2007. Upscaling hydraulic properties and soil water flow processes in heterogeneous soils. Vadose Zone Journal 6(1):1-28.

Appendix IV-A Tables

Table 11. Physical properties of length, bulk density, and porosity, and transducer log interval time for Flint sand hanging water columns.

Column Length (run number)	Bulk Density ($g\ cm^{-3}$)	Porosity ($m\ m^{-1}$)	Transducer Log Interval (s)
4.3 cm (R0)	1.74	0.34	1
14.4 cm (R7)	1.78	0.33	15
19.7 cm (R10)	1.78	0.33	30
23.8 cm (R5)‡	1.68	0.37	1
24.5 cm (R1)‡	†	†	1
24.9 cm (R11)	1.75	0.34	30
25.1 cm (R2)‡	1.62	0.39	1
29.5 cm (R3)	1.65	0.38	1
37.0 cm (R4)	1.63	0.39	1
43.3 cm (R8)	1.78	0.33	30
48.5 cm (R6)	1.74	0.34	1
55.0 cm (R9)	1.78	0.33	30

‡ Incomplete drainage set.

† Not measured.

Table 12. Range of capillary pressure, number of equilibrium steps, and total drainage time for Flint sand hanging water columns.

Column Length (run number)	Capillary Pressure Head Range (cm)	Equilibrium Steps	Total Drainage Time (h)
4.3 cm (R0)	0 - 41.7	16	5.0
14.4 cm (R7)	0 – 76.7	15	31.3
19.7 cm (R10)	0 – 59.6	16	74.6
23.8 cm (R5)‡	0 – 41.9‡	9‡	93.2‡
24.5 cm (R1)‡	0 – 43.1‡	12‡	5.1‡
24.9 cm (R11)	0 – 67.4	17	76.9
25.1 cm (R2)‡	0 – 47.2‡	16‡	11.3‡
29.5 cm (R3)	0 – 85.2	25	32.0
37.0 cm (R4)	0 – 66.3	22	47.3
43.3 cm (R8)	0 – 116.6	19	293.7
48.5 cm (R6)	0 – 123.9	20	191.8
55.0 cm (R9)	0 – 108.7	20	301.2

‡ Incomplete drainage set.

Table 13. Summary of Brooks and Corey (1964) model fits and estimates of the saturation (S), residual saturation S_r, air-entry value ψ_a, and pore-size distribution index λ fit to 1080 retention data points in Flint sand determined by neutron imaging (Kang et al, 2014).

S	S_r (Std Error)	ψ_a (Std Error) kPa	λ (Std Error)	RMSE
1.0	0.064 (0.024)	17.282 (0.062)	6.352 (0.262)	1.90×10^{-3}

Table 14. Summary of van Genuchten (1980) parameters predicted by the BC-vG Upscaler based on neutron point parameters and column length.

Column Length (run number)	S	S_r	α (kPa^{-1})	n	m	RMSE
4.3cm (R0)	1.001	0.065	0.051	11.942	0.916	6.70×10^{-3}
14.4cm (R7)	1.000	0.063	0.052	6.534	0.847	6.90×10^{-3}
19.7cm (R10)	0.999	0.062	0.054	5.132	0.805	1.14×10^{-2}
24.0cm (R11)	0.996	0.061	0.057	4.220	0.763	1.59×10^{-2}
29.5cm (R3)	0.992	0.060	0.060	3.650	0.726	2.02×10^{-2}
37.0cm (R4)	0.967	0.058	0.064	3.111	0.678	2.65×10^{-2}
43.3cm (R8)	0.921	0.058	0.062	2.980	0.664	2.73×10^{-2}
48.5cm (R6)	0.884	0.058	0.060	2.938	0.660	2.69×10^{-2}
55.0cm (R9)	0.845	0.058	0.056	2.912	0.657	2.59×10^{-2}

Table 15. Summary of van Genuchten (1980) parameters estimated from the measured average capillary pressure-saturation data for each Flint sand column.

Column Length (run number)	S (Std Err)	S_r (Std Err)	α (kPa^{-1}) (Std Err)	n (Std Err)	m (Std Err)	RMSE
4.3cm (R0)	1.000 (0.00)	0.115 (0.000)	0.046 (0.000)	9.133 (0.453)	0.890 (0.000)	6.56×10^{-3}
14.4cm (R7)	1.000 (0.000)	0.139 (0.000)	0.033 (0.000)	11.726 (1.380)	0.915 (0.000)	2.05×10^{-2}
19.7cm (R10)	1.000 (0.000)	0.064 (0.000)	0.038 (0.001)	6.726 (0.542)	0.851 (0.000)	1.94×10^{-2}
24.9cm (R11)	1.000 (0.000)	0.160 (0.000)	0.033 (0.001)	5.940 (0.456)	0.832 (0.000)	1.97×10^{-2}
29.5cm (R3)	1.000 (0.000)	0.104 (0.000)	0.034 (0.000)	5.915 (0.263)	0.831 (0.000)	1.98×10^{-2}
37.0cm (R4)	1.000 (0.000)	0.127 (0.000)	0.032 (0.000)	5.028 (0.300)	0.801 (0.000)	2.90×10^{-2}
43.3cm (R8)	1.000 (0.00)	0.110 (0.000)	0.027 (0.000)	4.951 (0.274)	0.798 (0.000)	1.97×10^{-2}
48.5cm (R6)	1.000 (0.000)	0.119 (0.00)	0.025 (0.000)	5.130 (0.337)	0.805 (0.000)	3.03×10^{-2}
55.0cm (R9)	1.000 (0.000)	0.097 (0.000)	0.023 (0.000)	4.824 (0.318)	0.793 (0.000)	3.58×10^{-2}

Table 16. Summary of van Genuchten (1980) parameters predicted by the BC-vG Upscaler algorithm based on neutron point parameters, column length, and a top reference for pressure.

Column Length (run number)	S	S_r	α (kPa^{-1})	n	m	RMSE
4.3cm (R0)	1.001	0.065	0.046	13.16	0.924	5.30×10^{-3}
14.4cm (R7)	1.000	0.064	0.038	8.790	0.886	2.90×10^{-3}
19.7cm (R10)	1.000	0.063	0.035	7.565	0.868	6.60×10^{-3}
24.9cm (R11)	1.000	0.063	0.032	6.743	0.852	1.01×10^{-2}
29.5cm (R3)	1.000	0.062	0.030	6.203	0.839	1.31×10^{-2}
37.0cm (R4)	0.999	0.062	0.028	5.582	0.821	1.76×10^{-2}
43.3cm (R8)	0.999	0.062	0.026	5.208	0.808	2.13×10^{-2}
48.5cm (R6)	0.999	0.061	0.025	4.957	0.798	2.40×10^{-2}
55.0cm (R9)	0.999	0.061	0.024	4.707	0.788	2.68×10^{-2}

Table 17. Summary of Brooks and Corey (1964) parameters of the saturation (S), residual saturation S_r, air-entry value ψ_a, and pore-size distribution index λ estimated by TrueCell (Jalbert et. al, 1999) from average capillary pressure-saturation data from nine columns of Flint sand. Neutron imaging point BC parameters are included for comparison.

Column Length (run number)	S	S_r	ψ_a (kPa)	λ
4.3cm (R0)	1.0	0.115	16.456	4.436
14.4cm (R7)	1.0	0.139	20.333	7.483
19.7cm (R10)	1.0	0.064	14.736	4.987
24.9cm (R11)	1.0	0.160	15.471	3.907
29.5cm (R3)	1.0	0.104	15.281	9.663
37.0cm (R4)	1.0	0.127	15.639	29.335
43.3cm (R8)	1.0	0.110	14.862	3.394
48.5cm (R6)	1.0	0.119	17.070	6.325
55.0cm (R9)	1.0	0.097	16.398	4.757
Neutron imaging	1.0	0.064	17.282	6.352

Appendix IV-B Figures

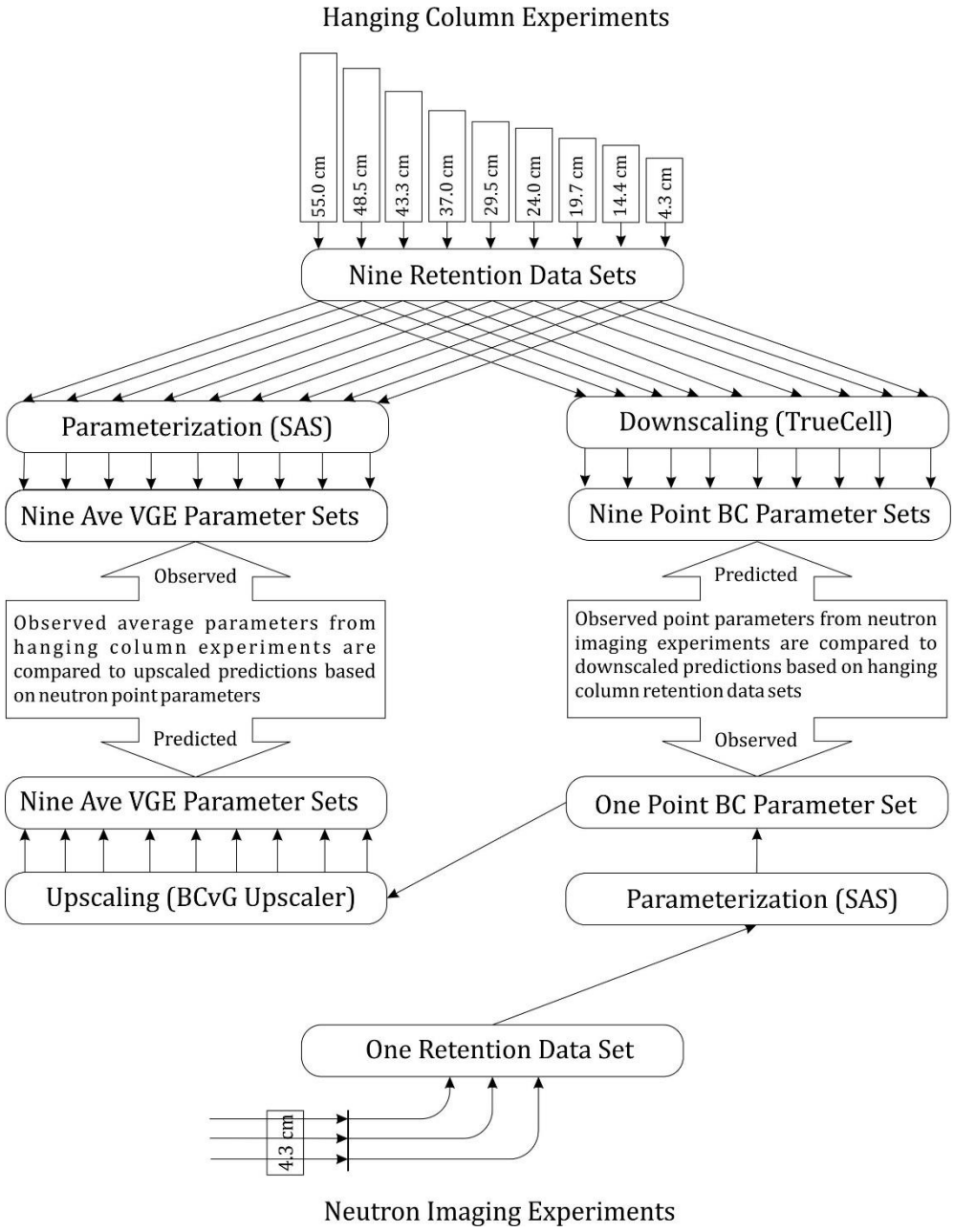


Figure 10. Conceptual diagram showing relationships between experimental data, data processing and parameterizations, and comparisons between experimental observations and predictions from analytical expressions.

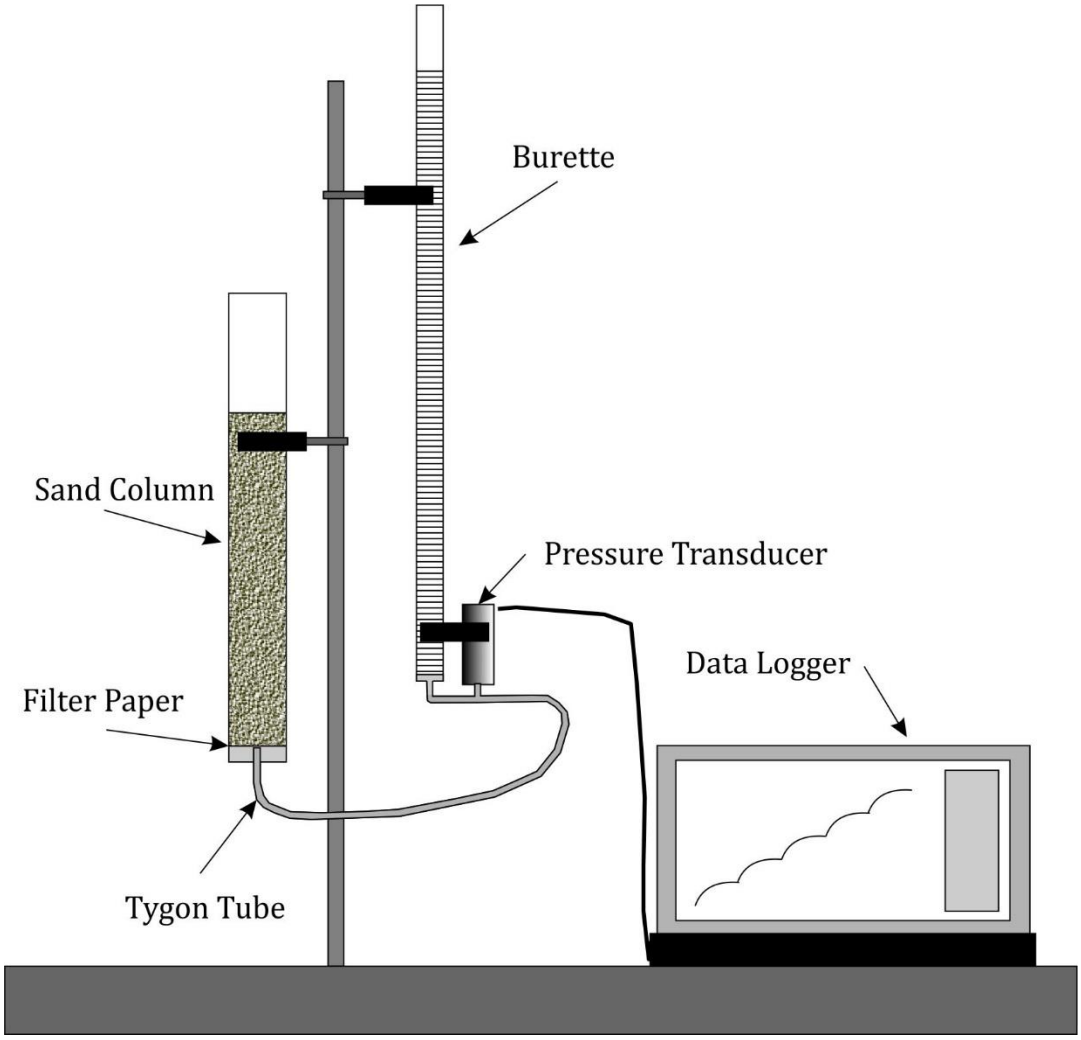


Figure 11. Hanging water column laboratory setup showing sand column, burette, pressure transducer, and data logging computer.

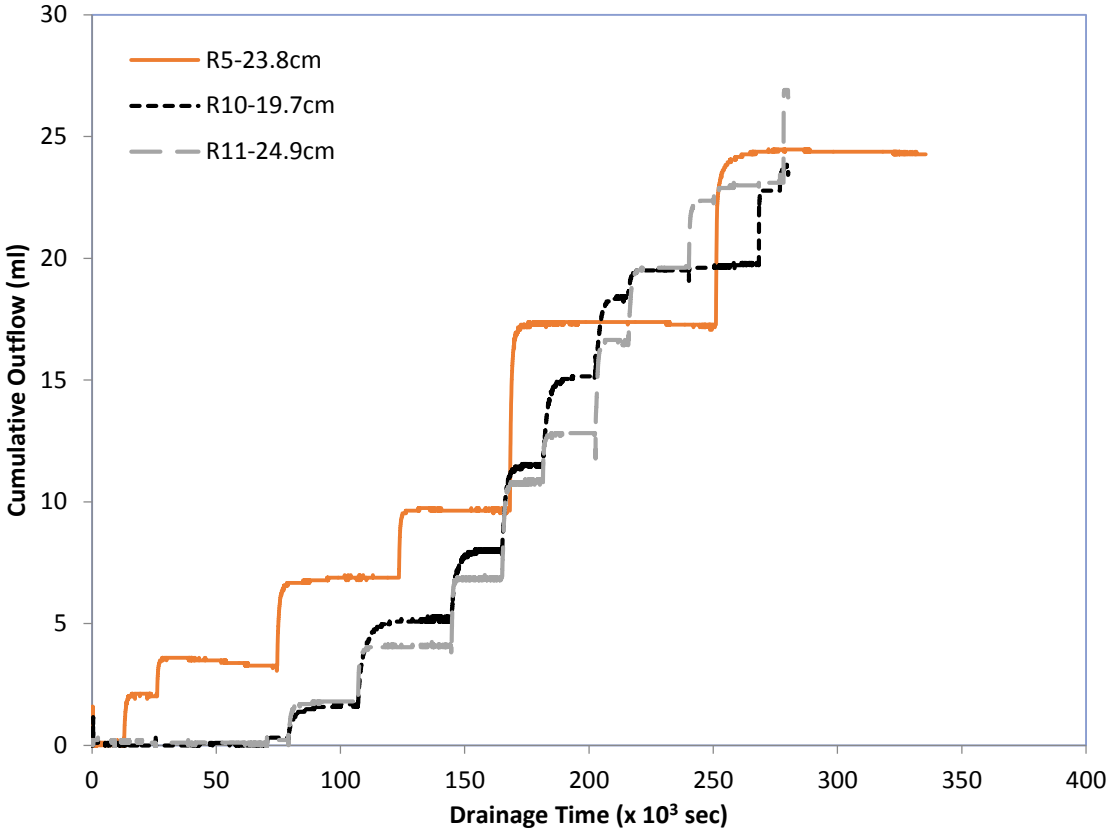


Figure 12. Cumulative water outflow through time for the 23.8 cm, 19.7 cm, and 24.9 cm Flint sand hanging water column drainage experiments.

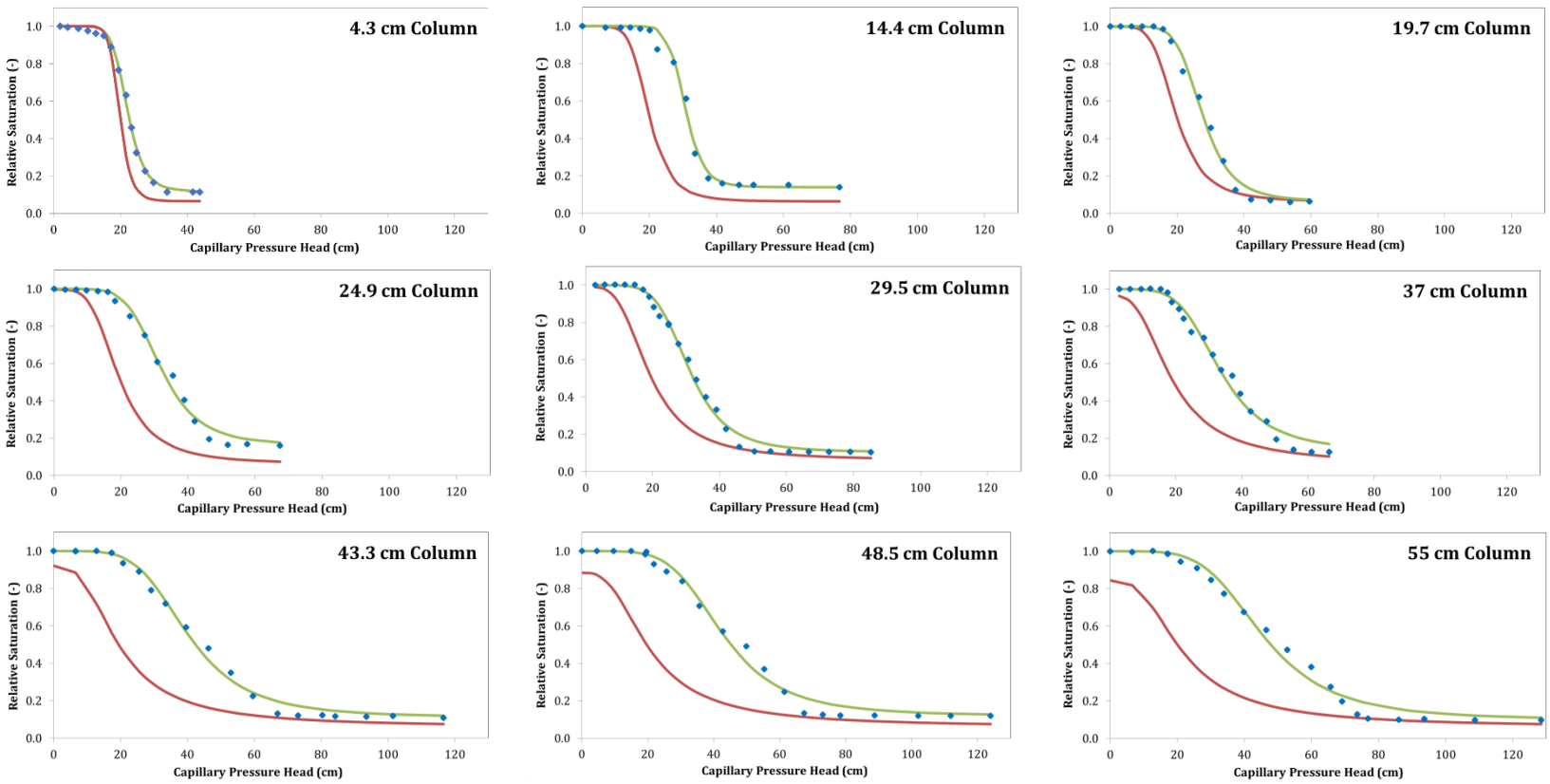


Figure 13. Comparison of upscaled predictions of capillary pressure-saturation functions (red) with measured average data points (blue) and van Genuchten (1980) functions fitted to measured average data points (green) for nine column lengths of Flint sand.

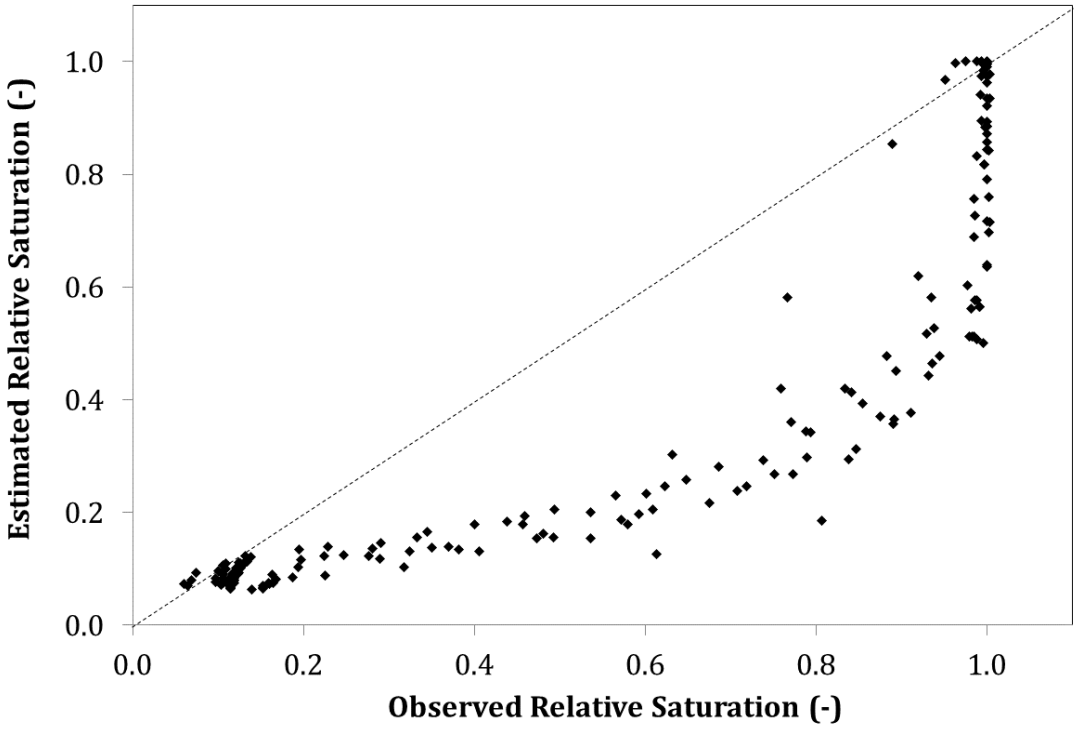


Figure 14. Relationship between observed relative saturation values and estimations of relative saturation in the van Genuchten (1980) capillary pressure-saturation equation predicted by the BC-vG Upscaler. The dashed line indicates a 1:1 correspondence.

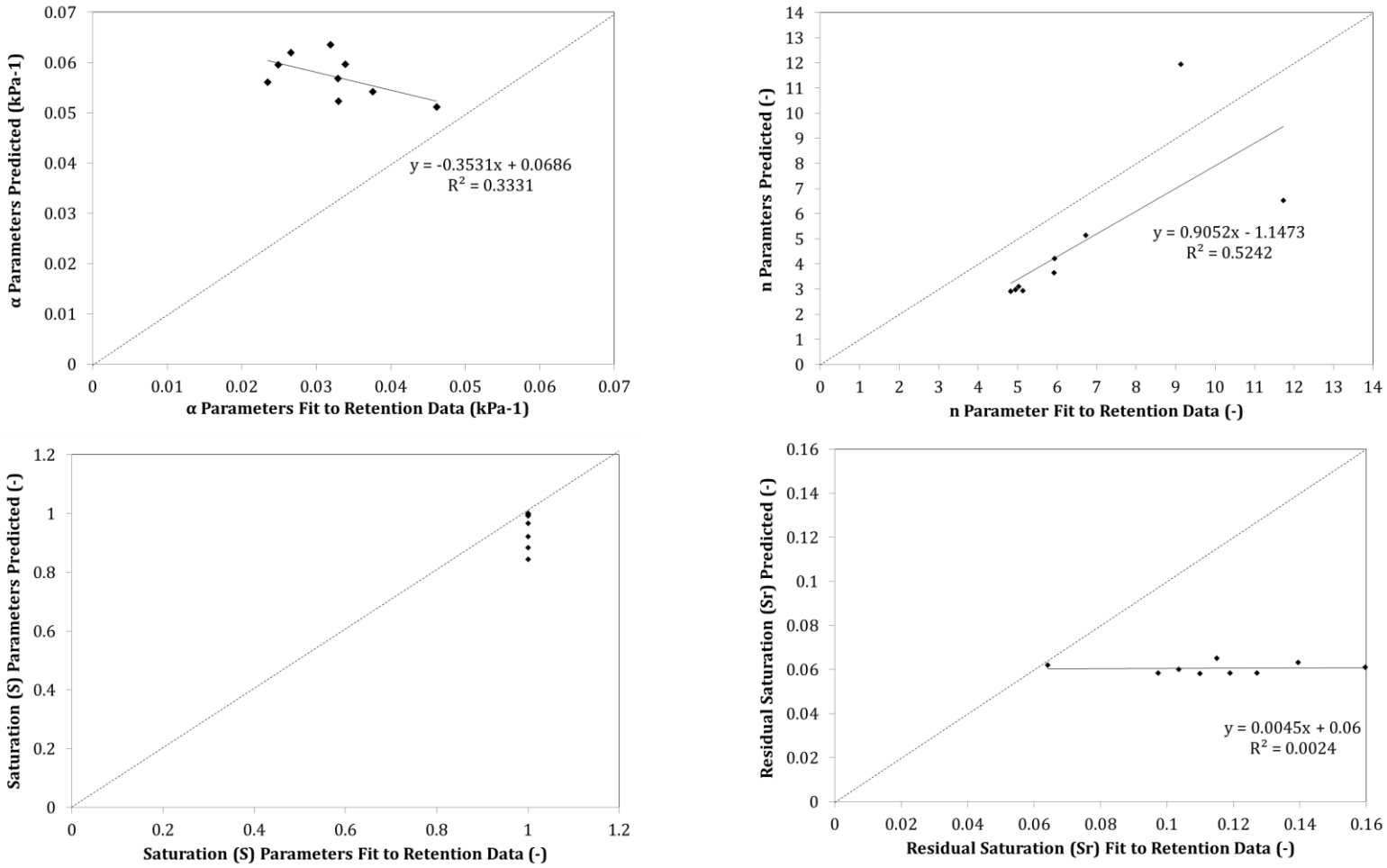


Figure 15. Relationship between *α* parameters, *n* parameters, residual saturation (S_r) values, and saturation values (S) in the van Genuchten (1980) capillary pressure-saturation equation predicted by the BC-vG Upscaler and fitted to the measured average drainage data. The dashed line indicates a 1:1 correspondence.

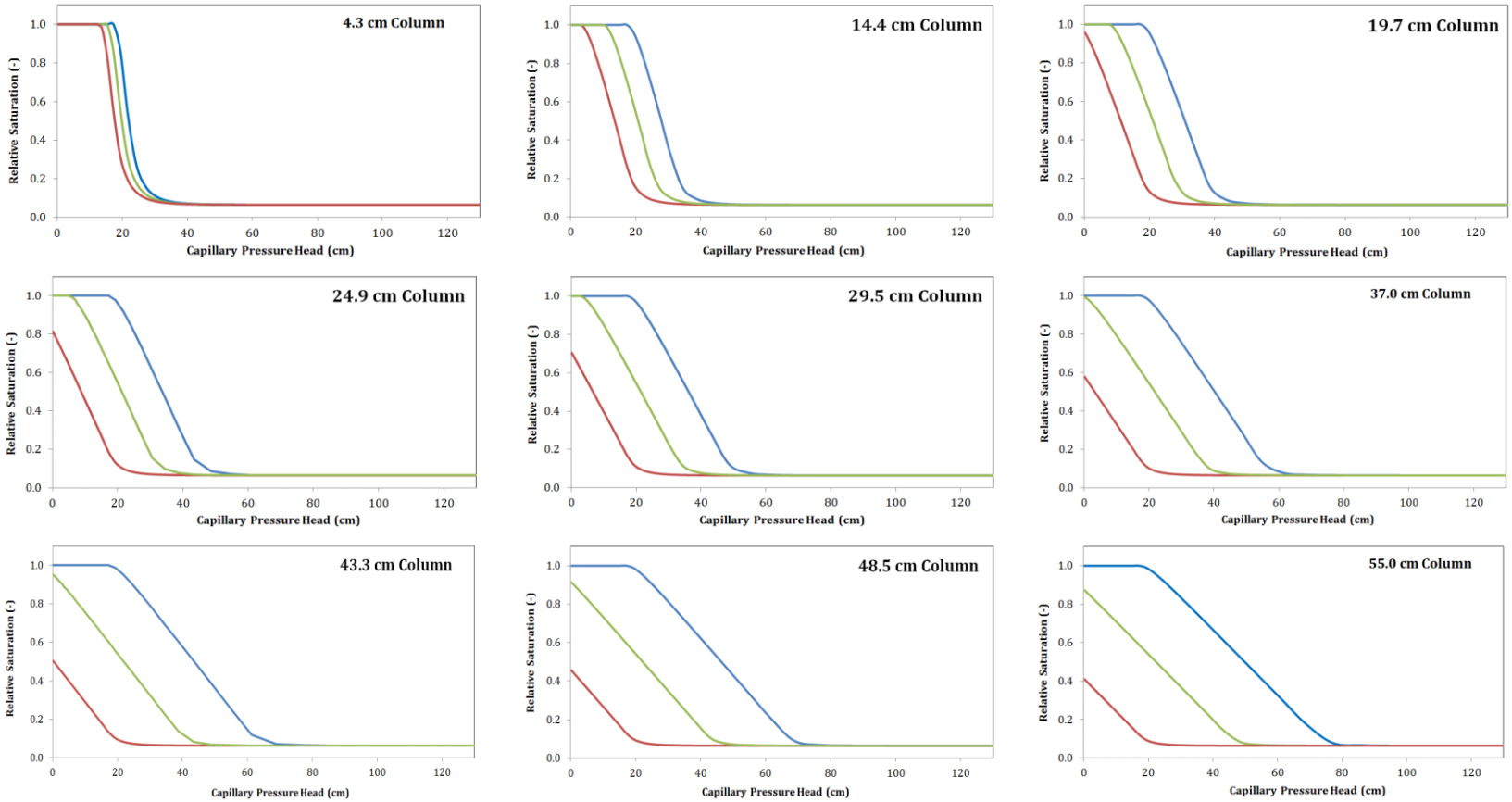


Figure 16. Comparisons of bottom (red), middle (green), and top (blue) pressure references on upscaled predictions of the capillary pressure-saturation functions for the nine column lengths.

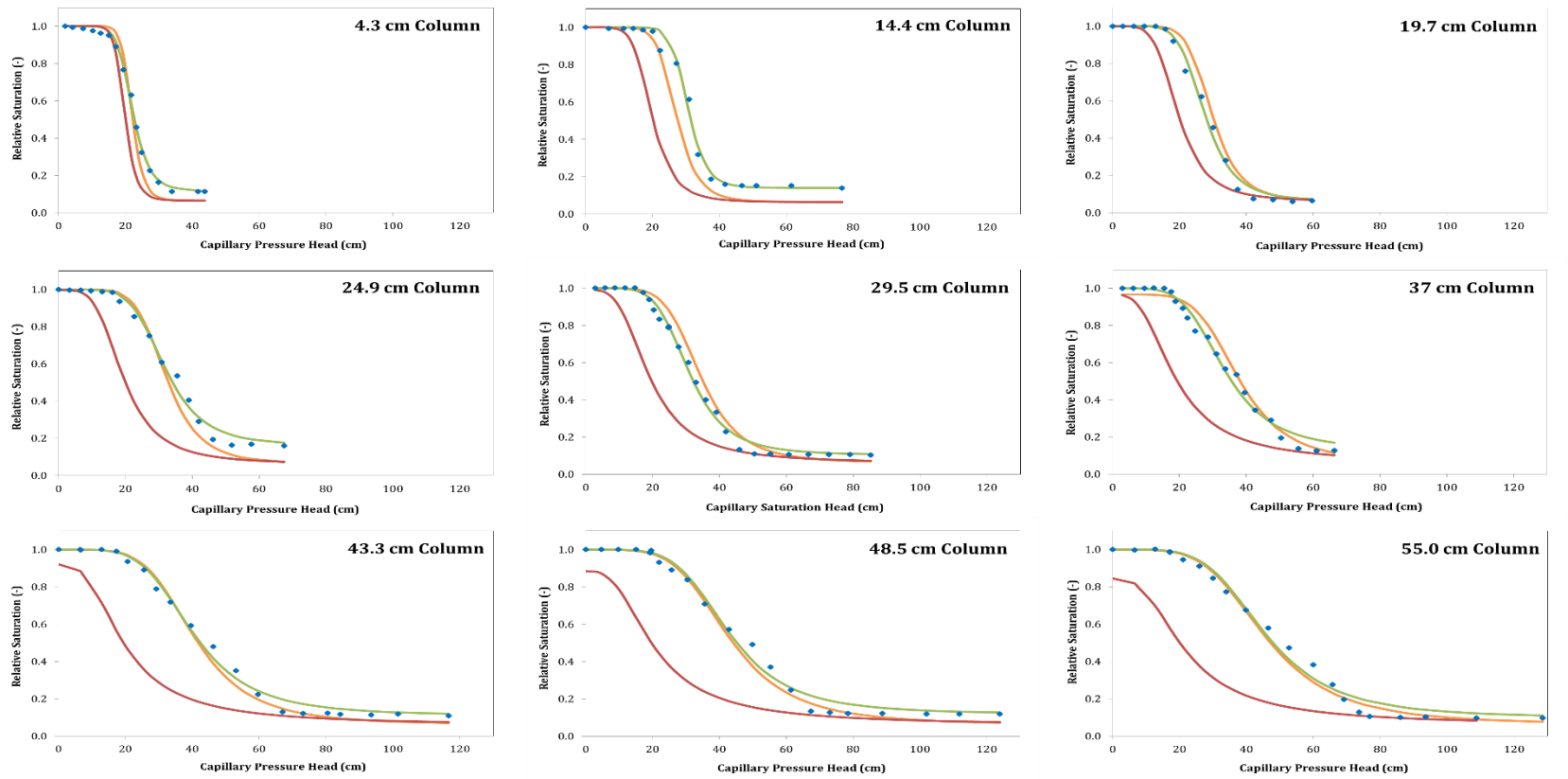


Figure 17. Upscaled top-pressure reference predictions of average capillary pressure saturation functions (orange) compared with measured average data points (blue) and van Genuchten (1980) functions fitted to measured average data points (green) for nine column lengths of Flint sand. Red lines are uncorrected mid-reference BCvG Upscaler predictions repeated here to for comparison with corrected top-reference BCvG Upscaler predictions.

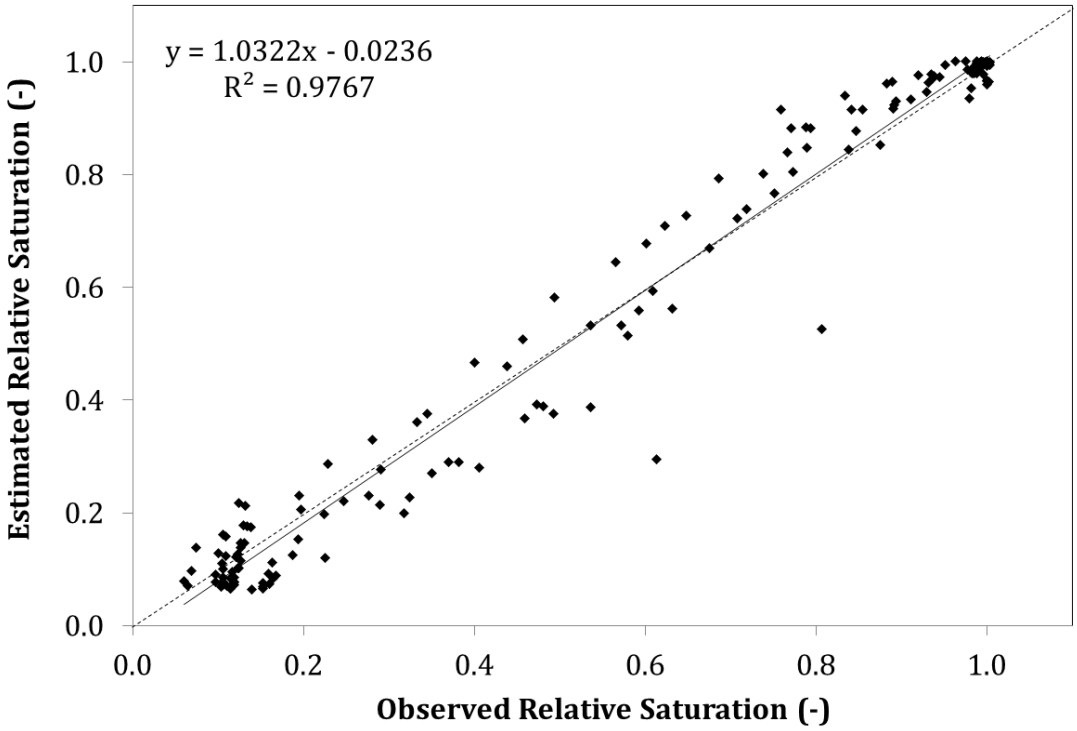


Figure 18. Relationship between observed relative saturation values and estimations of relative saturation in the van Genuchten (1980) capillary pressure-saturation equation predicted by the BC-vG Upscaler with the pressure reference at the column top. The dashed line indicates a 1:1 correspondence.

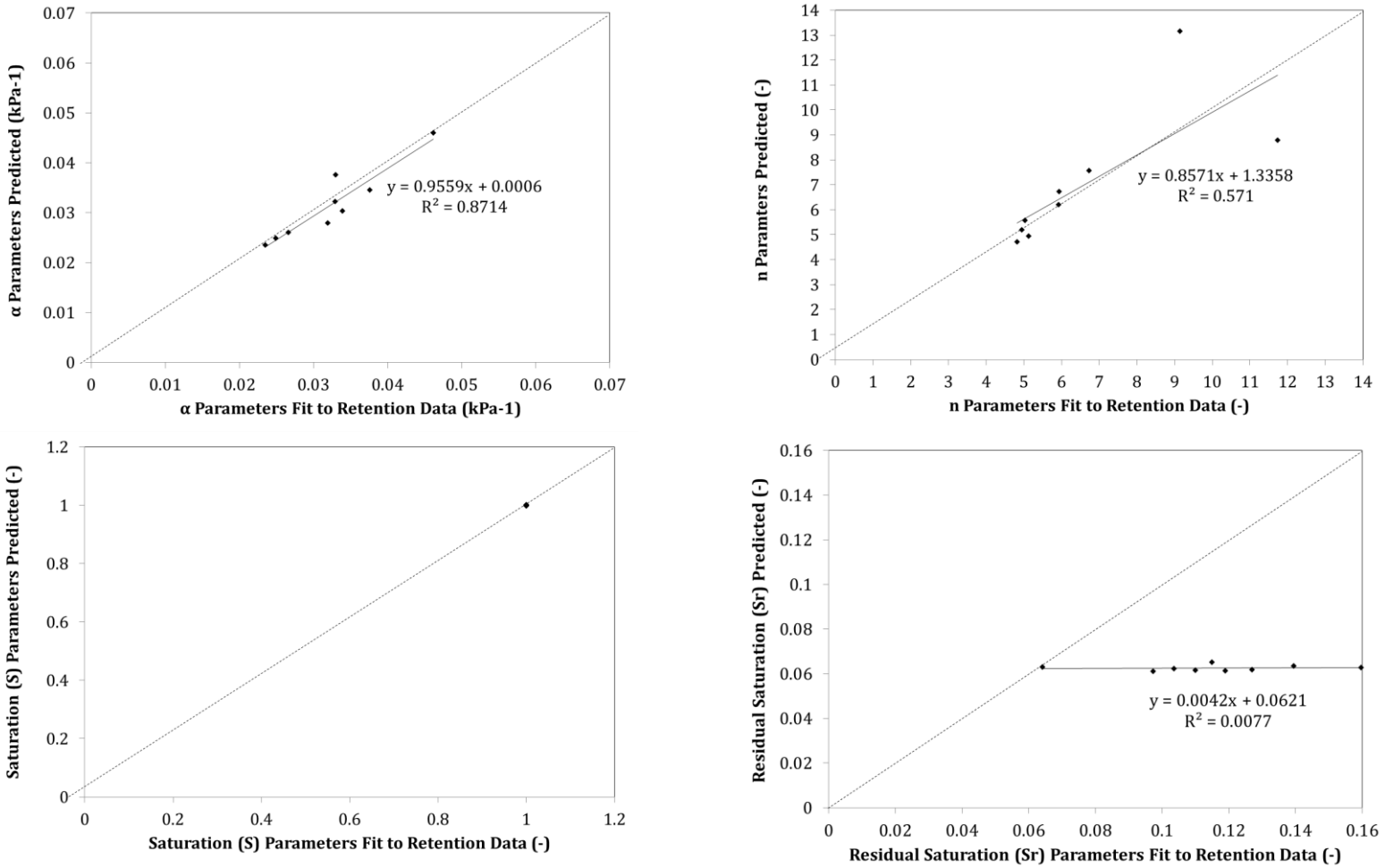


Figure 19. Relationship between α parameters, n parameters, residual saturation (S_r) values, and saturation values (S) in the van Genuchten (1980) capillary pressure-saturation equation predicted by the BC-vG Upscaler and fitted to the measured average drainage data. The dashed line indicates a 1:1 correspondence.

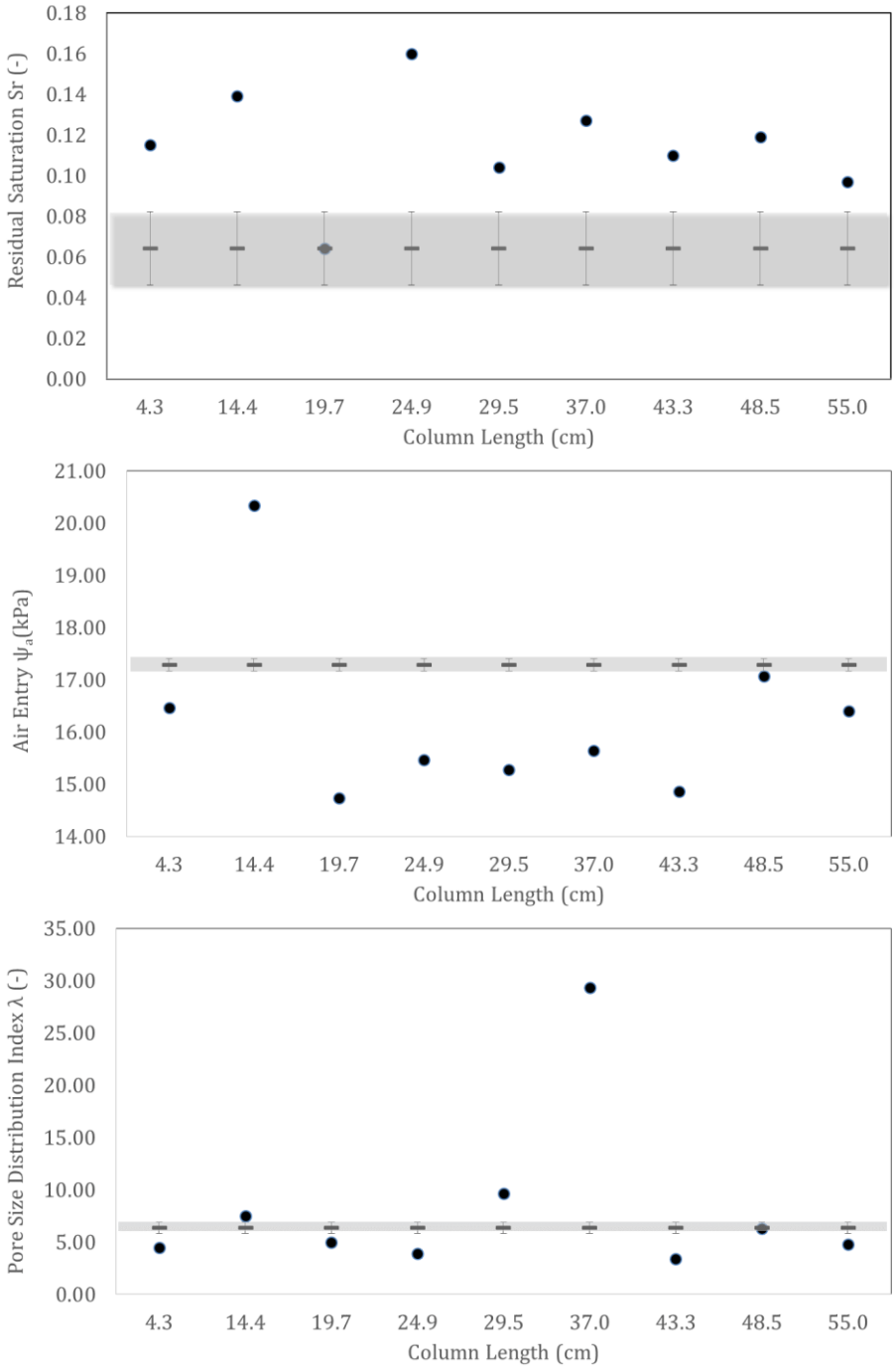


Figure 20. Relationship between TrueCell (Jalbert et. al, 1999) estimates of residual saturation (S_r) parameters, air entry (ψ_a) parameters, and pore size distribution index (λ) parameters shown as circles, and parameter values determined by neutron imaging. Neutron imaging values are shown as dashes with 95% confidence limits as error bars (gray).

Chapter V
Conclusions

Accurate characterization of the capillary pressure-saturation relationship in variably-saturated porous media is necessary for flow and transport modeling. This document has presented the results of three investigations into the relationship between point $S(\psi)$ and average $\langle S \rangle(\psi)$ functions. The emphasis has been on demonstrating the significance of using average versus point functions, demonstration of experimental techniques to measure point functions, and use of analytical expressions and computer programs to forward predict average functions or inversely extract point functions.

In Chapter II an integral computational method was applied to centrifuge drainage data to extract point $S(\psi)$ functions for a range of porous media including Berea sandstone, glass beads, and unconsolidated sediments. The resulting point $S(\psi)$ functions were then compared with average $\langle S \rangle(\psi)$ functions determined in the same materials. . The results show that the averaging method smoothes out the drainage process, yielding less steep capillary pressure - saturation functions relative to the corresponding point-based curves. Maximum deviations in saturation between the two methods ranged were significant (0.08 to 0.28). These discrepancies demonstrate that use of the average function instead of the point function could lead to modeling errors and inaccurate predictions of other hydraulic properties such as the relative permeability function. As a result of this work we recommended use of the integral method instead of the averaging method when determining the capillary pressure - saturation function by steady-state centrifugation.

In Chapter III a model scenario was created using the STOMP (Subsurface Transport Over Multiple Phases) numerical modeling tool for injection of supercritical CO_2 into a deep formation for long term geologic carbon sequestration. The model was used to compare the effect of using point and average functions on CO_2 injection flow rates and operating efficiency. Simulations using porosity, intrinsic permeability, and point van Genuchten parameters determined in Berea sandstone predicted mean flow rates 1.36 times higher than simulations using average capillary pressure-saturation function parameters in the same material holding all other

parameters constant. Use of the point function instead of the average function predicted significantly higher injection flow rates and therefore reduced cost per ton of CO_2 injected. Because of the lack of available research on the appropriate scale for the capillary pressure-saturation function in large-scale numerical simulations, we cannot say that the point parameter set produces a more accurate simulation compared to the average parameter set. However, this result highlights the importance of the scale effect on capillary pressure-saturation function parameters and its impact on the predictions of numerical models. Further research on the appropriate scale of these parameters for inclusion in large-scale simulations is needed.

In Chapter IV analytical expressions relating point and average functions were applied to drainage data from different length columns of Flint sand. Point functions determined directly in Flint sand by neutron imaging were upscaled using the BC-vG Upscaler to predict average functions for columns of nine different lengths of Flint sand ranging from 4.3 cm to 55.0 cm. The hanging column method was then used to measure average functions in Flint sand columns for the same lengths. The forward predictions of average functions were then compared to observed average functions. The comparisons show that upscaled functions were good predictions of observed average functions for the column lengths measured, but only if the pressure reference elevation for the upscale analysis is adjusted to the top of the column. The van Genuchten α parameters of the upscaled predictions correlate well with α parameters of measured retention functions after this adjustment, but upscaled predictions of residual saturation did not correspond with observed values even after the pressure reference was adjusted. The observed drainage data was also processed using TrueCell to inversely determine point functions from the observed data. Inverse predictions of point parameters from average retention data produced poor predictions of observed point function parameters measured by neutron imaging. Few parameters fell within the 95% confidence limits of the neutron estimates, and deviations were large for some column lengths. The discrepancy between the results

for the up- and down-scaling observed in this study may be related to the fact that the upscaling involved 9 independent predictions as compared to results for 9 different columns, each with their own experimental error, while the downscaling involved 9 independent predictions as compared to results for just 1 experimental column (i.e., no column-to-column variability).

Collectively this work has shown that there are measureable differences between average and point functions in the materials studied, and that those differences are significant in the context of numerical simulations. This work has also shown that point values can be upscaled to local scales up to 55 cm in Flint sand. The utility of upscaling most likely lies in its ability to scale point measurements up to representative scales for modeling purposes; it is left to future work to determine if this type of upscaling extends to the field scale. This work was not able to show that downscaling can predict point measurements from average measurements. The utility of downscaling, if shown to work in future work, lies most likely in its ability to convert easily measured average functions into point functions that can then be upscaled to other representative scales. Additional future work suggested by this research will be to determine why the BCvG Upscaler predicted significantly different residual saturations than were observed during the hanging column drainage experiments.

Vita

Clark Cropper is an Associate Professor of Geology at Volunteer State Community College (VSCC) in Gallatin Tennessee. He received a B.S. in Geology from Middle Tennessee State University (MTSU) in Murfreesboro, Tennessee and an M.S. in Geology from the University of Tennessee at Knoxville (UTK) in 1998. His graduate work focused on contaminant hydrogeology, supervised by Dr. Larry McKay. His thesis examined dense non-aqueous phase liquid flow through fractured clay-rich materials. After graduation, he worked for an environmental consulting firm in Middle Tennessee helping clients monitor and remediate leaking storage tanks.

Mr. Cropper made a career change to software development in 2001. He completed an M.S. in Computer Science at MTSU, studying software development, database administration, and software design. He then joined a software development firm where he helped develop online internet applications delivering real-time medical records to dialysis clinics. He was later promoted to software quality manager.

In 2004 Mr. Cropper made another career change. He taught computer literacy at MTSU and then joined the faculty of VSCC in 2005. In 2007 he began coursework for a Ph.D. in Geology in the Department of Earth and Planetary Science at UTK while also teaching at Volunteer State. His coursework focused on hydraulic properties of variably-saturated porous media supervised by Dr. Edmund Perfect. His current research is a comparison of point and average capillary pressure-saturation functions. He expects to complete his Ph.D. in December 2014 and return to teaching full time. Mr. Cropper currently resides in Gallatin, Tennessee with his wife Cheri, his daughter Grace, and his son Mason.